Scuola Internazionale Superiore di Studi Avanzati - Trieste

Phenomenology of the right-handed lepton mixings at the LHC in LR symmetric theory and the Time-Reversal symmetry violation in the $\mu \to e\gamma$ decay and $\mu \to e$ conversion process.

by

Juan Carlos Vasquez

—

A thesis submitted to the

Department of Theoretical Particle Physics of the

International School for Advanced Studies (SISSA) and the International Centre for Theoretical Physics (ICTP) in partial fulfillment

of the requirements for the degree of

Doctor of Philosophy

Department of Theoretical Particle Physics S.I.S.S.A

2016

SISSA - Via Bonomea 265 - 34136 TRIESTE - ITALY

Phenomenology of the right-handed lepton mixings at the LHC in LR symmetric theory and the Time-Reversal symmetry violation in the $\mu \to e\gamma$ decay and $\mu \to e$ conversion process.

by

Juan Carlos Vasquez

—

A thesis submitted to the

Department of Theoretical Particle Physics of the

International School for Advanced Studies (SISSA) and the International Centre for Theoretical Physics (ICTP) in partial fulfillment

of the requirements for the degree of

Doctor of Philosophy

Department of Theoretical Particle Physics S.I.S.S.A

2016

Vasquez, Juan Carlos (Ph.D., SISSA)

Phenomenology of the right-handed lepton mixings at the LHC in LR symmetric theory and the Time-Reversal symmetry violation in the $\mu \to e\gamma$ decay and $\mu \to e$ conversion process.

Advisor: Prof. Goran Senjanović

Co-Advisor: Prof. Stefano Bertolini

We study how the elements of the leptonic right-handed mixing matrix can be determined at the LHC in the minimal Left-Right symmetric extension of the standard model. We do it by explicitly relating them with physical quantities of the Keung-Senjanović process and the lepton number violating decays of the right doubly charged scalar. We also point out that the left and right doubly charged scalars can be distinguished at the LHC, without measuring the polarization of the final state leptons coming from their decays. Then we study time reversal symmetry violation in the $\mu \to e\gamma$ decay and the $\mu \to e$ conversion process and compute a T-odd triple vector correlation for the $\mu \to e\gamma$ decay and the $\mu \to e$ conversion process, finding simple results in terms of the CP violating phases of the effective Hamiltonians. Finally we focus on the minimal Left-Right symmetric extension of the Standard Model, which is a complete model of neutrino masses that can lead to an appreciable correlation. We show that under rather general assumptions, this correlation can be used to discriminate between Parity or Charge-conjugation as the discrete Left-Right symmetry.

Dedication

To Barbara and Adrian

Acknowledgements

I would like to thank Goran Senjanović for all his teachings, guidance and most importantly for being such a great advisor and for spending a big portion of his time teaching me. I really appreciate it. He has tough me from the smallest details, to the not so small datails such as how to write correctly, but perhaps the most important thing I learned from him, is that science is about the search of the truth. In the future, it will be my main guide on how to proceed in every aspect of my life. Thanks are also given to Stefano Bertolini and Goran Senjanović for all the enlightening discussions during these years that in the end give as a product this thesis. Thanks are also given to both of them for spending their time in correcting the manuscripts of my works that helped me in learning the craft of writing a scientific paper.

Contents

Chapter

1 Introduction **1**

2 The minimal Left-Right symmetric model **5**

2.1 Lower bounds on the LR scale and particle masses 10

2.2 The Dirac mass matrix from the heavy and light neutrino Majorana masses in the minimal left-right model 11

2.3 Lepton Flavor violation. Experimental Limits 13

2.4 The $\mu \to e\gamma$ decay and $\mu \to e$ conversion process. Theory and effective Hamiltonians 15

2.4.1 $\mu \to e\gamma$ decay. Effective Hamiltonian 15

2.4.2 $\mu \to e$ conversion. Theory and Effective Hamiltonian 15

2.4.3 Total conversion rate 18

2.4.4 Triple vector correlation in the conversion process 19

3 Right-handed lepton mixings at the LHC **23**

3.1 Determination of the right-handed leptonic mixing matrix 23

3.1.1 Keung-Senjanović process 24

3.1.2 Yukawa couplings of the triplet scalars in the LR model 38

3.1.3 Decays of the doubly-charged scalar δ_R^{++} 40

4 Time-reversal symmetry violation in several Lepton-Flavor-Violating processes **44**

4.1 Computation of a triple vector correlation in the $\mu \to e\gamma$ decay 44

4.2 Computation of a triple vector correlation in the $\mu \to e$ conversion process 46

4.3 Triplet vector correlations in the minimal Left-Right theory 48

4.3.1 $\mu \to e\gamma$ decay 48

4.3.2 $\mu \to e$ conversion process 53

5 Conclusions **56**

Appendix

A Scalar potential of the minimal LR model **59**

B Mass reach for Z_R at the LHC with 13 TeV of center of mass energy **61**

C Expressions for the Dirac phase δ in the right-handed leptonic mixing matrix **63**

D Cross sections values **65**

E Branching ratio formulas for $\delta_R^{++} \to l^+ l^+$ **67**

F Kinematics of the $\mu \to e\gamma$ process and the triple vector correlation **68**

Bibliography **70**

Tables

Table

2.1 Best fit values for the neutrino oscillation parameters for normal (NH) and inverted (IH) neutrino mass spectrum. 14

2.2 Experimental limits on the muon LFV decays 15

3.1 Conditions that the maximal/minimal mixing angles should satisfy in terms of the final states for the KS process for two heavy neutrinos at the LHC. 29

3.2 Conditions that lead to the maximal CP violation from the phase δ for the two heavy neutrinos at the LHC. 30

3.3 Conditions that the maximal/minimal mixing angles should satisfy in terms of the final states for the KS process for three heavy neutrinos at the LHC. 35

3.4 Conditions that lead to the maximal CP violation from the phase δ for the three heavy neutrinos at the LHC. 36

D.1 Cross sections for the different processes considered for two heavy neutrinos at the LHC in the normal hierarchy (NH) neutrino mass spectrum and for different values of the lightest heavy neutrino mass. 65

D.2 Cross sections for the different processes considered for three heavy neutrinos at the LHC in the normal hierarchy (NH) neutrino mass spectrum and for different values of the lightest heavy neutrino mass. 66

D.3 Cross sections for the different processes considered for three heavy neutrinos at the LHC in the inverted hierarchy (IH) neutrino mass spectrum and for different values of the lightest heavy neutrino mass. 66

Figures

Figure

2.1 Reference frame and the setup for the $\mu \to e\gamma$ decay and the $\mu \to e$ conversion process. 21

3.1 Keung-Senjanović process in both opposite-sign leptons (Left) and the lepton-number-violating same-sign leptons in the final state (Right). 24

3.2 Plots for the quantities R_1,R_2,R_τ and R_4 in the type II see-saw dominance ($V_L \propto V_R^*$) as a function of the lightest neutrino mass eigenstate for 2 heavy neutrinos at the LHC in the NH case. Red dots with errors bars are the results obtained by taking into account the hadronization effects using Pythia 6. We assume the values of the gauge boson $m_{W_R} = 3$ TeV and the heavy neutrino mass $m_{N_2} = 1$ TeV 31

3.3 Number of events (scaled to one) as a function of the ratio E_H/E_E between the Hadronic energy E_H and the electromagnetic energy E_E for the two hardest jets in energy ($E(j_1) > E(j_2)$) coming from the process $p + p \to W_R^\pm \to N_1 e^\pm \to e^\pm e^\pm + jj$ together with the main SM backgrounds. We assume $m_{W_R} = 3$ TeV and $m_{N_1} = 100$ GeV, $m_{N_2} = 2$ TeV and $m_{N_3} = 2$ TeV. The generic label V stands for the gauge bosons W or Z. 33

3.4 Plots for the quantities R_1,R_2,R_3 and R_4 in the type II see-saw dominance ($V_L \propto V_R^*$) as a function of the lightest neutrino mass eigenstate for 3 heavy neutrinos at the LHC in the NH case. Red dots with errors bars are the results obtained by taking into account the hadronization effects using Pythia 6. We assume the values of the gauge boson $m_{W_R} = 3$ TeV and the heavy neutrino mass $m_{N_2} = 0.17$ TeV 36

3.5 Plots for the quantities R_1,R_2,R_3 and R_4 in the type II see-saw dominance ($V_L \propto V_R^*$) as a function of the lightest neutrino mass eigenstate for 3 heavy neutrinos at the LHC in the IH case. Red dots with errors bars are the results obtained by taking into account the hadronization effects using Pythia 6. We assume the values of the gauge boson $m_{W_R} = 3$ TeV and the heavy neutrino mass $m_{N_2} = 0.95$ TeV 37

3.6 Pair production of the doubly charged scalars with Z/γ^* as intermediate states. . . . 40

3.7 Plots for the branching ratios of δ_R^{++} into leptons in the (ϕ_2, ϕ_3) plane. We assume $\delta = \pi/2$ and the masses for the heaviest and lightest right-handed neutrinos, $m_{heaviest} = 1$TeV and $m_{lightest} = 0.5$TeV in type II dominance. (Left) Br($\delta_R^{++} \to e^+e^+$). (Center) Br($\delta_R^{++} \to e^+\mu^+$). (Right) Br($\delta_R^{++} \to \mu^+\mu^+$). (top) Normal hierarchy for neutrino masses. (Bottom) Inverted hierarchy for neutrino masses. 42

3.8 Production cross sections for a pair of doubly charged scalars at LHC with 13 TeV center of mass energy as a function of their masses M_Δ. Red line corresponds to δ_R^{++} and blue lines to δ_L^{++} production cross sections. Gray bands show the theoretical uncertainties. 43

4.1 Plot of the loop function $S_3(x)$. 50

4.2 Plot obtained by considering the MEG bound shown in Eq. (1.1). (Right) Normal hierarchy case (NH). (Left) Inverse hierarchy case (IH). The colored region is the allowed one. (Top) Mass of the heaviest right-handed neutrino $m_{N_H} = 0.5$ TeV. (Bottom) Mass of the heaviest right-handed neutrino $m_{N_H} = 1$ TeV. 50

4.3 (Top) Contour plots illustrating the absolute value of the asymmetry defined in (4.7) as a function of the lightest neutrino mass m_{N_0} and the Dirac phase δ for $\mathcal{P}$ as the LR symmetry. (Bottom) Contour plots illustrating the value of the asymmetry defined in (4.7) as a function of the lightest neutrino mass m_{N_0} and the Dirac phase δ (assuming $\phi_\mu - \phi_e = 0$) for $\mathcal{C}$ as the LR symmetry. (Left) Normal hierarchy for neutrino masses. (Right) Inverse hierarchy for neutrino masses. We take the gauge boson mass $m_{W_R} = 6$TeV, the heaviest right-handed neutrino mass $m_{N_H} = 1$TeV and common masses for the doubly charged scalars of $m_\delta = 1$ TeV. The mixing angles are $\theta_{12} \simeq 33.6^o$, $\theta_{23} \simeq 41.9^o$, $\theta_{13} \simeq 8.7^o$. 52

4.4 Plot obtained by considering the SINDRUM II bound for Titanium shown in Eq. (1.2). (Right) Normal hierarchy case (NH). (Left) Inverse hierarchy case (IH). The colored region is the allowed one. We take the mass of the heaviest right-handed neutrino $m_{N_H} = 1$ TeV. 54

B.1 Probability density as a function of the isolation cut R. 62

B.2 Values of the integrated luminosity $\mathcal{L}_{\text{int}}$ (fb^{-1}) necessary to produce 10 events as a function of the Z_R mass in TeV. Error bars for $\mathcal{L}_{\text{int}}$ are also shown in the plot. 62

Chapter 1

Introduction

The minimal left-right model (LR) has been proposed more than four decades ago [1, 2, 3, 4, 5] in order to explain the maximal parity violation observed in weak interactions and more recently established as a complete model of neutrino masses and mixings [6]. It introduces three new heavy gauge bosons W_R^+, W_R^-, Z_R and the heavy neutrino states N. In this model, the maximally observed parity non conservation is a low energy phenomenon, which ought to disappear at energies above the W_R mass. Furthermore, the smallness of neutrino masses is related to the near maximality of parity violation [7, 8, 9], through the seesaw mechanism [7, 8, 9, 10, 11, 12]. Historically it has been know that there are two kinds of LR symmetry, namely generalized parity ($\mathcal{P}$) or charge conjugation ($\mathcal{C}$) (for reviews see [13, 14, 15]) and to our knowledge, there have not been any proposal that try to experimentally distinguish between these two cases. In this thesis we have something to say about this issue, as we shall see in the next sections.

It turns out that there exists [16] an exciting decay of W_R into two charged leptons and two jets ($W_R \to l + N \to ll + jj$). We refer to it as the Keung-Senjanović (KS) process. This process has a small background and no missing energy. It gives a clean signal for the W_R production at LHC, as well as probing the Majorana nature of the heavy neutrinos. Since there is no missing energy in the decay, the reconstruction of the W_R and N invariant masses is possible. If true, the Majorana mass of N will lead to the decay of the heavy neutrino into a charged lepton and two jets ($N \to l + jj$), with the same probability of decaying into a lepton or antilepton.

The production of W_R is ensured at the LHC because in the quark sector the left and right

mixing matrices are related. For $\mathcal{C}$ as the Left-Right symmetry, the mixing angles are exactly equal, therefore the production rate of W_R is not suppressed. For $\mathcal{P}$ the situation is more subtle and needed an in-depth study. Finally in [17] a simple analytic expression valid in the entire parameter space was derived for the right-handed quark mixing matrix. It turns out that despite parity being maximally broken in nature, the Right and Left quark mixing matrices end up being very similar. Moreover the hypothesis of equal mixing angles can be tested at the LHC by studying the hadronic decays of W_R [18].

In the Leptonic sector the connection between the Left and Right leptonic mixing matrices goes away, since light and heavy neutrino masses are different. For $\mathcal{C}$ as the Left-Right symmetry, the Dirac masses of neutrinos are unambiguously determined in terms of the heavy and light neutrino masses [6]. Light neutrino masses are probed by low energy experiments, whereas the ones of the heavy neutrinos can be determined at the LHC. This is why the precise determination of the right-handed leptonic mixing matrix, one of the main topic of this thesis, is of fundamental importance. As we shall see all the three mixing angles and three of CP violating phases may be determined by studying the final states in the KS process and decays of the doubly charged scalars. Furthermore we point out that these two processes are not sensitive to three of the phases appearing in V_R, unlike electric dipole moments of charged leptons.

The other main topic of this thesis is time-reversal symmetry violation in the $\mu \to e\gamma$ decay and the $\mu \to e$ conversion process and we focus in these two particular processes due to the expected improvements in the sensitivity –see [15] for a detailed review of LFV processes. More precisely, we find analytical expression for the asymmetry in both processes and using the most general effective Hamiltonians.

The MEG collaboration reports the best experimental limit for the $\mu \to e\gamma$ decay [19]

$$\mathbf{Br}(\mu \to e\gamma) \equiv \frac{\Gamma(\mu \to e\gamma)}{\Gamma(\mu \to e\nu_\mu\nu_e)} < 5.7 \times 10^{-13} \tag{1.1}$$

and the SINDRUM II collaboration gives the strongest limits for the $\mu \to e$ conversion process,

namely [20],

$$\mathbf{Br}(\mu + \mathrm{Ti(Au)}) \to e + \mathrm{Ti(Au)}) \equiv \frac{\Gamma(\mu \to e)}{\Gamma_{\mathrm{capt}}} < 6.1(7) \times 10^{-13}, \tag{1.2}$$

where Γ_{capt} is the muon capture rate in the vicinity of a nucleus. Upgrades of ongoing experiments have been considered with the final goal of achieving a sensitivity around $10^{-18} - 10^{-19}$ [21, 22, 23, 24]. Given the current limits and the future improvements, there exist the possibility of having enough statistics to start probing CP violation beyond the SM in the next round of experiments. This is suggested and studied in [25, 26].

We focus on quantities that test T violation in the absence of final-state interactions and among these quantities are triple vector correlations made up of the momenta or spins of the participating particles [27]. In [28], it is suggested that triplet vector correlations can be used to probe CP violation in the $\mu \to e$ conversion process. Here we present the first analytical computation for the correlation suggested in [28] for the $\mu \to e$ conversion process and we extend their work in two ways: first, we compute the correlation for the $\mu \to e\gamma$ decay and second we include the full set of effective operators that enter the $\mu \to e$ conversion process.

This thesis is mainly based on the works presented in [29, 30]. In chapter 2 we give an introduction to the minimal LR model including the relevant sector and interactions in the discussion to follow. Then we also introduce the relevant theoretical tools needed when computing the T asymmetries in the $\mu \to e\gamma$ decay and the $\mu \to e$ conversion process. The results obtained are presented in the two main chapters 3 and 4. More precisely, In chapter 3 we present a complete strategy to determine the three mixing angles and three phases in the mixing matrix of heavy neutrinos. For this strategy, the KS process and the decay of the right type doubly charged scalar play the fundamental role. Later in chapter 4 we present the result of an analytical computation of a triple vector asymmetry in the $\mu \to e\gamma$ decay and the $\mu \to e$ conversion process, as well as some phenomenological discussion in the context of the minimal LR model. It turns out that these asymmetries can be used to discriminate between parity or charged conjugation as the LR symmetries in the most interesting scenario. For the computation we make use the general effective

Hamiltonians and further restricting them when discussing their implications within the LR model. Finally in chapter 5 we present our conclusions.

Chapter 2

The minimal Left-Right symmetric model

Parity maximally broken in the SM is one of its most puzzling features and the minimal Left-Right symmetric model [1, 2, 3, 4, 5] was proposed in order to account for this issue. In this model parity is assumed to be spontaneously broken at high energies, therefore if the symmetry breaking scale is sufficiently low, we might be able to observed parity restoration in high energy processes. As a consequence of the LR symmetry, this model predicted massive neutrinos long before their masses were established by oscillation experiments. More recently it was also established as a complete model of neutrino masses and mixings [6], namely it does to neutrino masses what the SM does for the quarks and charged leptons masses. Furthermore, the smallness of neutrino masses is related to the near maximality of parity violation [7, 8, 9], through the seesaw mechanism [7, 8, 9, 10, 11, 12].

The gauge group: The minimal Left-Right symmetric model [1, 2, 3, 4, 5] is based on the gauge group $\mathcal{G} = SU(2)_L \times SU(2)_R \times U(1)_{B-L}$, with an additional discrete symmetry that may be generalized parity ($\mathcal{P}$) or charge conjugation ($\mathcal{C}$).

The discrete Left-Right symmetry: there are two possible left-right symmetries that may be parity or generalized charge conjugation. Under the discrete left-right symmetry the fields transform as follows:

$$\mathcal{P}: \begin{cases} \mathcal{P} f_{(L,R)} \mathcal{P}^{-1} = \gamma_0 f_{(R,L)} \\ \mathcal{P}\Phi\mathcal{P}^{-1} = \Phi^\dagger \\ \mathcal{P}\Delta_{(L,R)}\mathcal{P}^{-1} = -\Delta_{(R,L)} \end{cases} \qquad \mathcal{C}: \begin{cases} \mathcal{C} f_{(L,R)} \mathcal{C}^{-1} = C(\bar{f}_{(R,L)})^T \\ \mathcal{C}\Phi\mathcal{C}^{-1} = \Phi^T \\ \mathcal{C}\Delta_{(L,R)}\mathcal{C}^{-1} = -\Delta^*_{(R,L)} \end{cases} \tag{2.1}$$

where γ_μ ($\mu = 0, 1, 2, 3.$) are the gamma matrices and C is the charge conjugation operator. One

important question one may ask is how distinguished between $\mathcal{P}$ or $\mathcal{C}$ as the LR symmetry. As we shall see in the next sections, CP asymmetries in the low energy LFV decays such as $\mu \to e\gamma$ and $\mu \to e$ conversion are of special interest.

Quarks and Leptons: quarks and leptons are assigned to be doublets in the following irreducible representations of the gauge group:

$$q_L = \begin{pmatrix} u \\ d \end{pmatrix}_L : (2, 1, \frac{1}{3}), \quad q_R = \begin{pmatrix} u \\ d \end{pmatrix}_R : (1, 2, \frac{1}{3}), \tag{2.2}$$

$$L_L = \begin{pmatrix} \nu \\ l \end{pmatrix}_L : (2, 1, -1), \quad L_R = \begin{pmatrix} N \\ l \end{pmatrix}_R : (1, 2, -1). \tag{2.3}$$

N represents the new heavy neutrino states, whose presence play a crucial role in explaining the smallness of the neutrino masses on the basis of the see-saw mechanism.

The Higgs sector: the scalar sector consists in one bidoublet Φ, in the (2,2,0) representation of $\mathcal{G}$ and two scalar triplets Δ_L and Δ_R [7, 8], belonging to (3,1,2) and (1,3,2) representation respectively

$$\Phi = \begin{pmatrix} \phi_1^0 & \phi_1^+ \\ \phi_2^- & \phi_2^0 \end{pmatrix}, \quad \Delta_{L,R} = \begin{pmatrix} \delta_{L,R}^+/\sqrt{2} & \delta_{L,R}^{++} \\ \delta_{L,R}^0 & -\delta_{L,R}^+/\sqrt{2} \end{pmatrix}. \tag{2.4}$$

. The expression for the more general scalar potential consistent with the LR symmetry may be found elsewhere [8, 31, 32, 15, 33, 34, 35, 36] and we give its expression in appendix A for completeness.

Symmetry breaking: At the first stage of symmetry breaking, the Higgs field Δ_R takes a v.e.v (v_R) along its neutral component and breaks the Left-Right symmetry down to the standard model gauge group. At this stage the bidoublet Φ, breaks the electroweak gauge group down to $U(1)_{em}$ and from the interactions in the scalar potential, Δ_L gets an induced small vev $v_L \propto v^2/v_R$ (v is the electroweak v.e.v).

The v.e.v's of the Higgs fields may be written as [9]

$$\langle \Phi \rangle = \begin{pmatrix} v_1 & 0 \\ 0 & v_2 e^{i\alpha} \end{pmatrix}. \tag{2.5}$$

$$\langle \Delta_R \rangle = \begin{pmatrix} 0 & 0 \\ v_R & 0 \end{pmatrix}, \quad \langle \Delta_L \rangle = \begin{pmatrix} 0 & 0 \\ v_L e^{i\theta_L} & 0 \end{pmatrix} \tag{2.6}$$

where $v_L \ll v_1^2 + v_2^2 \ll v_R^2$, since it can be shown from the minimization conditions of the potential that $v_L \propto v^2/v_R$.

If the mixing with the right handed triplet scalar field is neglected the physical mass eigenstates that belong to the bidoublet Φ are of the form:

$$h = \frac{1}{v}\Re e(v_1\phi_1^0 + v_2 e^{ia}(\phi_2^0)^*) \tag{2.7}$$

$$H = \frac{1}{v}\Re e(-v_2\phi_1^0 + v_1 e^{ia}(\phi_2^0)^*) \tag{2.8}$$

$$A = \frac{1}{v}\Im m(-v_2\phi_1^0 + v_1 e^{ia}(\phi_2^0)^*) \tag{2.9}$$

$$H^+ = \frac{1}{v}(v_1\phi_1^+ + v_2 e^{ia}\phi_2^+) \tag{2.10}$$

Notice that the mixing among the two triplets Δ_L and Δ_R is suppressed by the v.e.v v_L and hence they are physical fields to a very good aproximation.

Lepton masses: lepton masses are due to the following Yukawa interactions (once the Higgs fields take their v.e.v along their neutral components)

$$\begin{aligned} \mathcal{L}_Y = \quad & \bar{L}_L(Y_\Phi \Phi + \tilde{Y}_\Phi \tilde{\Phi}) L_R + \tfrac{1}{2}(L_L^T C i\sigma_2 Y_{\Delta_L} \Delta_L L_L \\ & + L_R^T C i\sigma_2 Y_{\Delta_R} \Delta_R L_R) + h.c., \end{aligned} \tag{2.11}$$

where $\tilde{\Phi} = \sigma_2 \Phi^* \sigma_2$, σ_2 is the Pauli matrix and $C \equiv i\gamma_2\gamma_0$.

Invariance of the Lagrangian under the Left-Right symmetry requires the Yukawa couplings

to satisfy

$$\mathcal{P}: \begin{cases} Y_{\Delta_{R,L}} = Y_{\Delta_{L,R}} \\ Y_\Phi = Y_\Phi^\dagger \\ \tilde{Y}_\Phi = \tilde{Y}_\Phi^\dagger \end{cases}, \quad \mathcal{C}: \begin{cases} Y_{\Delta_{R,L}} = Y_{\Delta_{L,R}}^* \\ Y_\Phi = Y_\Phi^T \\ \tilde{Y}_\Phi = \tilde{Y}_\Phi^T \end{cases} \tag{2.12}$$

Consistent with the above notation, the neutrino mass interaction terms are of the form [8, 9]

$$\mathcal{L}_\nu = \frac{1}{2}\nu_L^T Y_{\Delta_L} v_L C \nu_L + \frac{1}{2}(N_L^c)^T C M_N N_L^c + (N_L^c)^T C M_D^\dagger \nu_L + h.c. \tag{2.13}$$

and the neutrino masses take the see-saw form [8]

$$M_N = Y_{\Delta_R}^* v_R, \tag{2.14}$$

$$M_\nu = Y_{\Delta_L} v_L e^{i\theta_L} - M_D^\dagger \tfrac{1}{M_N} M_D^*, \tag{2.15}$$

$$M_D = v_1 Y_\Phi + \tilde{Y}_\Phi v_2 e^{-i\alpha} \tag{2.16}$$

The charged lepton mass matrix is

$$M_l = Y_\Phi v_2 e^{i\alpha} + \tilde{Y}_\Phi v_1 \tag{2.17}$$

α is called the "spontaneous" CP phase. All the physical effects due to θ_L, can be neglected, since this phase is always accompanied by the small v_L.

As usual, the mass matrices can be diagonalized by the bi-unitary transformations

$$\begin{aligned} M_l = U_{lL} m_l U_{lR}^\dagger, \quad M_D = U_{DL} m_D U_{DR}^\dagger, \\ M_\nu = U_\nu^* m_\nu U_\nu^\dagger, \quad M_N = U_N^* m_N U_N^\dagger, \end{aligned} \tag{2.18}$$

where m_l, m_ν and m_N are diagonal matrices with real, positive eigenvalues.

Charged gauge interactions with leptons: from the covariant derivative and in the mass eigenstate basis the flavor changing charged current Lagrangian is

$$\mathcal{L}_{cc} = \frac{g}{\sqrt{2}}(\bar{\nu}_L V_L^\dagger \not{W}_L l_L + \bar{N}_R V_R^\dagger \not{W}_R l_R) + h.c., \tag{2.19}$$

V_L and V_R are the left and right leptonic mixing matrices respectively

$$V_L = U_{lL}^{\dagger} U_{\nu}, \tag{2.20}$$

$$V_R = U_{lR}^{\dagger} U_N. \tag{2.21}$$

We may use the freedom of rephasing the charged lepton fields to remove three unphysical phases from V_L, which ends up having 3 mixing angles and 3 phases, namely one Dirac and two Majorana phases. On the other hand since the freedom of rephasing the charged lepton is already used for V_L, its right-handed analogue –the leptonic mixing matrix V_R– is a general 3×3 unitary matrix and may be therefore parametrized by 3 mixing angles and 6 phases. As it is well known, the mixing angles of V_L mixing matrix are probed by low energy experiments. Instead we focus in the precise determination of the mixing angles and phases of its right-handed analogue V_R at hadron colliders. This matrix has in general 3 different angles and 6 phases –as discussed above– and we write it in the form $V_R = K_e \hat{V}_R K_N$, where $K_e = \mathrm{diag}(e^{i\phi_e}, e^{i\phi_\mu}, e^{i\phi_\tau})$, $K_N = \mathrm{diag}(1, e^{i\phi_2}, e^{i\phi_3})$ and

$$\hat{V}_R = \begin{pmatrix} c_{13}c_{12} & c_{13}s_{12} & s_{13} \\ -s_{12}c_{23}e^{i\delta} - c_{12}s_{13}s_{23} & c_{12}c_{23}e^{i\delta} - s_{12}s_{13}s_{23} & c_{13}s_{23} \\ s_{12}s_{23}e^{i\delta} - c_{12}s_{13}c_{23} & -c_{12}s_{23}e^{i\delta} - s_{12}s_{13}c_{23} & c_{13}c_{23} \end{pmatrix}, \tag{2.22}$$

$s_{\alpha\beta}(c_{\alpha\beta})$ is the short-hand notation for $\sin\theta_{\alpha\beta}(\cos\theta_{\alpha\beta})$ with $\alpha, \beta = 1, 2, 3$.

Doubly charged scalar interactions with leptons: the next relevant interactions for our discussion are the ones between the charged leptons and the doubly charged scalars

$$\mathcal{L}_{\Delta} = \tfrac{1}{2} l_R^T C Y'_{\Delta_R} \delta_R^{++} l_R + \tfrac{1}{2} l_L^T C Y'_{\Delta_L} \delta_L^{++} l_L + h.c., \tag{2.23}$$

$$Y'_{\Delta_R} = \tfrac{g}{m_{W_R}} V_R^* m_N V_R^{\dagger}. \tag{2.24}$$

If $\mathcal{C}$ is the left-right symmetry, is easy to see from Eqs. (2.1) and (2.11) that [13, 14, 15]

$$Y'_{\Delta_L} = (Y'_{\Delta_R})^*. \tag{2.25}$$

For parity ($\mathcal{P}$) the situation is different since for a non-zero spontaneous phase the charged lepton masses are not hermitian. Then after the symmetry breaking, one would expect that the left and right Yukawa interactions with the doubly-charged scalar are not the same. It turns out that for right-handed neutrinos masses accessible at the LHC, the charged lepton mass matrices end up being almost hermitian [37]. Let us notice that it implies that Yukawa couplings of the doubly charge scalars must satisfy[1]

$$Y^{'}_{\Delta_L} = S_l Y^{'}_{\Delta_R} S_l + i \tan\beta \sin\alpha (R^* Y^{\prime}_{\Delta_R} S_l + S_l Y^{\prime}_{\Delta_R} R^{\dagger}) + \mathcal{O}\left[(\tan\beta \sin\alpha)^2\right] \tag{2.26}$$

with

$$(R)_{ij} = \frac{(M^{\prime}_D)_{ij}}{(m_l)_i + (m_l)_j} - \frac{1}{2}\tan\beta e^{-i\alpha}(S_l)_{ij}. \tag{2.27}$$

Where S_l is a 3×3 matrix with $\pm$ signs in the diagonal entries and zero otherwise, $M^{\prime}_D = U^{\dagger}_{lL} M_D U_{lR}$ and $\beta \equiv v_2/v_1$. This is obtained in analogy to the approach used for the quark mixing matrix in [17, 38], where it is also shown that $\tan 2\beta \sin\alpha \lesssim 2m_b/m_t$. Hence one can safely assume that $Y^{'}_{\Delta_L} \backsimeq Y^{'}_{\Delta_R}$ as a leading order approximation in the most interesting scenario.

Notice that (2.24) depends on the Majorana phases and therefore the decay rates of δ^{++}_R into two leptons in the final state depend in a CP-even way on the Dirac and Majorana phases. As we shall see in the next sections, this fact can be used to determine some of the phases in V_R at the LHC.

2.1 Lower bounds on the LR scale and particle masses

Theoretical bounds on the Left-Right scale were considered in the past and historically the small $K_L - K_S$ mass difference gives a lower bound on the Left-Right-scale of around 3 TeV in the minimal model [39][2] . More recently in [41], an updated study and a complete gauge invariant computation of the K_L, K_S and B_d, B_s meson parameters, gives $m_{W_R} > 3.1(2.9)$ TeV for $\mathcal{P}(\mathcal{C})$. In [42] it is claimed that for parity as the Left-Right symmetry, the θ_{QCD} parameter, together with

[1] See section 3.1.2 for a detailed derivation of this relation

[2] For recent updates see references [32, 40]

K-meson mass difference Δm_K, push the mass of W_R up to 20 TeV [41, 42]; however this depends on the UV completion of the theory. Direct LHC searches, on the other hand, gives in some channels a lower bound of around 3 TeV [43, 44]. For the Z_R gauge boson there exist the theoretical bound from the relation $m_{Z_R} \simeq 1.7 m_{Z_R}$. In appendix B we show an analysis in which the expected sensitivity to the Z_R boson mass is obtained. We find that the mass reach of the LHC for 300fb^{-1} (1000fb^{-1}) of integrated luminosity is around 5.5 TeV (7.2 TeV) approximately – see Fig. B.2.

The more recent and stringent bounds on the heavy scalar particles that belong to the bidoublet comes form the K meson system and give the lower bound for the H, H^+, A heavy scalars masses of around $15 - 20$ TeV [40, 41].

Direct LHC bounds on the doubly charged scalars are around 400 GeV and 500 GeV to δ_L^{++} and δ_R^{++} respectively [45]. More recently in [34] theoretical bounds were obtained. It was concluded from the sum rules for the mass differences among the Δ_L components, together with the oblique parameters, that in order to observed the Δ_L at the LHC the W_R is then far out of its reach. Conversely were the W_R mass 3 TeV, the δ_L^0 mass would have to be greater than 6 TeV. Since the α_3 coupling present in the potential give the mass to heavy scalars H, H^+, A, it is clear that in order to have a low scale W_R mass of few TeV the α_3 coupling should not be small. For instance for W_R mass of 6 TeV $\alpha_3 \simeq 4.8$ –e.g. see Eq. 12 in [34]. In this case and as shown in [34], the enhanced α_3 coupling would contribute to the Higgs mass through the δ_R^{++} loop. Therefore a lower correlated mass bound with W_R emerges, which disfavor both accessible at the LHC but still some borderline space remain –see Fig. 7 in [34]. Lower bounds on the Higgs particle $\Re e(\delta_R^0)$ responsible for the generation of the LR scale and the Majorana heavy neutrino masses have not been obtained so far.

2.2 The Dirac mass matrix from the heavy and light neutrino Majorana masses in the minimal left-right model

In this section we describe the parametrization for the Dirac mass term presented in [46], which essentially states that in the general case of type I plus type II see-saw mechanism, the Dirac mass cannot be determined in terms of the heavy and light neutrino masses. Later we describe

following [6] how within the LR model this is not an issue.

Consider the Majorana mass for neutrinos,

$$M_\nu = Y_{\Delta_L} v_L e^{i\theta_L} - M_D^\dagger \frac{1}{M_N} M_D^*. \tag{2.28}$$

Assume now that the elements of M_ν and $Y_{\Delta_L} v_L e^{i\theta_L}$ are all known. Remember that the elements of M_ν can be probed in neutrino oscillation experiments whereas $Y_{\Delta_L} v_L e^{i\theta_L}$ can be probed in the decays of the scalars belonging to the left triplet Δ_L into SM gauge bosons W and Z – see [47, 48] for detailed studies on this subject. In this case there exist an unitary matrix U such that

$$U^T \left(M_\nu - Y_{\Delta_L} v_L e^{i\theta_L} \right) U = D = -U^T M_D^\dagger \frac{1}{M_N} M_D^* U, \tag{2.29}$$

where D is a diagonal matrix. Multiplying both sides by $\sqrt{D^{-1}}$ one gets

$$1 = -D^{-\frac{1}{2}} U^T M_D^\dagger \frac{1}{M_N} M_D^* U D^{-\frac{1}{2}} = O^\dagger O^*, \tag{2.30}$$

from which it follows that M_D is given by

$$M_D = i\sqrt{M_N^*} O \sqrt{D^*} U^T \tag{2.31}$$

and we see that even if we completely know the light and heavy neutrino masses, the Dirac mass is determined up to an arbitrary complex orthogonal matrix. It is worth to emphasize that the elements of an arbitrary, complex, orthogonal matrix are not bounded –in contrast to the case of real orthogonal matrices– and could be as large as one wants, hence rendering the Dirac mass matrix elements arbitrary.

It turns out that within the LR model M_D is completely determined in terms of the heavy and light neutrino masses and in this respect $\mathcal{C}$ as the LR symmetry plays the fundamental role [6]. In what follows we present and derive the main result presented in [6] and to this end consider Eq. 2.16 with $M_D = M_D^T$, namely

$$M_\nu = Y_{\Delta_L} v_L e^{i\theta_L} - M_D^* \frac{1}{M_N} M_D^*, \tag{2.32}$$

from which one can find the expression of M_D that is given by [6]

$$M_D^* = -iM_N\sqrt{M_N^{-1}(M_\nu - Y_{\Delta_L}v_L e^{i\theta_L})} = -iM_N\sqrt{M_N^{-1}M_\nu - \frac{v_L}{v_R}e^{i\theta_L}}. \quad (2.33)$$

Finally comparing Eq. 2.31 with 2.33 one finds that the matrix O is fixed and given by

$$O^* = \sqrt{M_N}\sqrt{M_N^{-1}(M_\nu - Y_{\Delta_L}v_L e^{i\theta_L})}U\sqrt{D^{-1}} = \sqrt{m_N}\sqrt{m_N^{-1}V_R^T V_L^* m_\nu}\sqrt{m_\nu^{-1}} + \mathcal{O}(\tfrac{v_L}{v_R}), \quad (2.34)$$

which shows that the matrix O is completely fixed in terms of the light and heavy neutrino masses and mixings. This is our main motivation for studying the right handed leptonic mixings and phases at the LHC, since as can be seen from the above equation, the determination of V_R is paramount importance in order to determine the Dirac masses of neutrinos and test the Higgs mechanism for neutrino masses. Notice that the matrix elements of O are bounded and naturally of order one –as already emphasized in [6].

2.3 Lepton Flavor violation. Experimental Limits

The SM predicts massless neutrinos and it implies that the "flavor" number associated to every neutrino is conserved separately at the tree level [3] . This is so because due to its masslessness, one can freely rotate the neutrinos in the mass eigenstate basis of charged leptons in such a way as to make the mixing matrix between charged leptons and neutrinos proportional to the identity. However in the neutrino sector non zero mass differences and its associated Lepton Flavor Violation (LFV) have been observed in the form of neutrino oscillations by the Super-Kamiokande [52], SNO [53], KamLAND [54] and other more recent experiments experiments, so it is clear the the SM must be modified in order to account for massive neutrinos. Therefore one would think that LFV processes are not forbidden and could be observed at sizable rates, this is no so for charged leptons and the reason is that the neutrino mass scale is much smaller than electroweak scale. Recent

[3] Violated at the quantum level by anomalies [49, 50] that lead to Lepton and Baryon number violation in the SM at negligible rates [51].

bounds coming from cosmological considerations give a bound on the sum of neutrino masses of $\sum m_\nu \leq 0.23$ eV [55] and there are also bounds to their mass differences coming from oscillation experiments. In table 2.1 we show the best fit values for the oscillation parameters shown in [56], where it may be seen that the neutrino mass differences ranges from 10^{-5} eV^2 to 10^{-3} eV^2. Notice that the mixing angles are large, so what is really producing the suppression of the flavor-violating effects for charged leptons is the disparity between the neutrino mass scale and the electroweak scale.

	Best fit value	3σ range
$\sin^2\theta_{12}$	0.302	$0.267 \to 0.344$
θ_{12}°	33.36	$31.09 \to 35.89$
$\sin^2\theta_{23}$	0.413	$0.342 \to 0.667$
θ_{23}°	40.0/50.4	$35.8 \to 54.8$
$\sin^2\theta_{13}$	0.0227	$0.0156 \to 0.0299$
θ_{13}°	8.66	$7.19 \to 9.96$
$\delta(^\circ)$	300	$0 \to 360$
$\frac{\Delta m^2_{21}}{10^{-5}eV^2}$	7.5	$7.00 \to 8.09$
$\frac{\Delta m^2_{31}}{10^{-3}eV^2}$ (NH)	2.473	$2.276 \to 2.695$
$\frac{\Delta m^2_{32}}{10^{-3}eV^2}$ (IH)	-2.427	$-2.469 \to$ -2.242

Table 2.1: Best fit values for the neutrino oscillation parameters for normal (NH) and inverted (IH) neutrino mass spectrum.

In the SM the $\mu \to e\gamma$ decay rate is more than 50 order of magnitude smaller that the standard muon decay rate into one electron and two neutrinos. The point is that this situation is completely different if new physics beyond the SM is introduced. For instance in the minimal LR model there are new contributions to the $\mu(\tau) \to e\gamma$ decay and $\mu \to e$ conversion at sizable rates. In Table 2.2 we show the experimental bounds for the main muon LFV decays considered in the experiments as well as current experiments that are expected to give new improved limits in the near future. Our main focus in this thesis is devoted to the $\mu \to e\gamma$ decay and $\mu \to e$ conversion process. The $\mu \to eee$ decay is planned to be studied in the near future.

Finally limits on the LFV processes of tau leptons are much weaker and around 10^{-8} [57, 58, 59, 60, 61]. The expected improvement in these limits are most likely to be around 10^{-9} [62, 63].

Decay Channel	Experiment	Branching ratio limit	Upgraded sensitivity (next data acquisition)
$\mu \to e\gamma$	MEG	5.7×10^{-13} [19]	5×10^{-14} [64]
$\mu + Ti(Au) \to e + Ti(Au)$	SINDRUM II	$6.1(7) \times 10^{-13}$[20]	10^{-14}[65, 66]
$\mu \to eee$	SINDRUM	1×10^{-12}[67]	10^{-16}[68]

Table 2.2: Experimental limits on the muon LFV decays

2.4 The $\mu \to e\gamma$ decay and $\mu \to e$ conversion process. Theory and effective Hamiltonians

In the following sections we give some theoretical tools we used when computing the $\mu \to e\gamma$ decay and the $\mu \to e$ conversion process.

2.4.1 $\mu \to e\gamma$ decay. Effective Hamiltonian

The $\mu \to e\gamma$ decay is predicted to be negligible small in the SM with massive neutrinos, therefore if this process is seen it implies that new physics is behind it. The effective Hamiltonian for this process is of the form

$$H_{eff} = \frac{4eG_F m_\mu}{\sqrt{2}} \bar{e}(p_e)\sigma_{\mu\nu}F^{\mu\nu}(A_L P_L + A_R P_R)\mu(p_\mu) + h.c., \tag{2.35}$$

where e is the electromagnetic coupling constant, $F_{\mu\nu}$ is the electromagnetic field strength for the photon field, G_F is the Fermi constant, $P_{(R,L)} \equiv \frac{1}{2}(1 \pm \gamma_5)$, m_μ is the muon mass and $e(p_e)$ and $\mu(p_\mu)$ are the spinors for the electron and muon respectively. For this process we use the gamma matrices in the Weyl basis and the coefficients A_L and A_R are calculated within a given physical model.

2.4.2 $\mu \to e$ conversion. Theory and Effective Hamiltonian

Theoretical studies of this process were performed in the past [69, 70, 71, 72]. In [72] the outgoing electron coming from the conversion process, belongs to one of the states in the continuum energy spectrum for the Coulomb potential and as a matter of fact the outgoing electron must be treated as a plane wave. One way to argue this is by noticing that an electron in the continuum

energy spectrum, is described by a Dirac spinor in the angular momentum basis. Experimentally, the detected electron has a definite 4-momentum implying that is must be treated as a plane wave.

In this work we present a method for computing a triple vector correlation that tests T-violation in the $\mu \to e$ conversion process for various nuclei. We make use of the formalism developed in [73].

We use the following representation for the γ matrices

$$\gamma_0 = \beta = \begin{pmatrix} 1 & 0 \\ 0 & -1 \end{pmatrix}, \qquad \gamma_i = \begin{pmatrix} 0 & \sigma_i \\ -\sigma_i & 0 \end{pmatrix}, \tag{2.36}$$

and

$$\sigma_{\mu\nu} = \frac{i}{2}[\gamma_\mu, \gamma_\nu], \qquad \gamma_5 = -i\gamma_1\gamma_2\gamma_3\gamma_0, \tag{2.37}$$

where the σ_i are the Pauli matrices where $i = 1, 2, 3$ and the index μ takes the values $\mu = 0, 1, 2, 3$.

The Dirac's equation for the central field problem in polar coordinates is given by (the energy is given in units of the electron mass)

$$E\psi = H\psi = [-i\gamma_5\Sigma_r(\frac{\partial}{\partial r} + \frac{1}{r} - \frac{\beta}{r}K) + V + \beta]\psi, \tag{2.38}$$

where

$$\Sigma_r = \frac{1}{r}\sum_i \Sigma_i, \quad \Sigma_i = \frac{i}{2}[\gamma_j, \gamma_k] \qquad (\{\text{i,j,k}\} \text{ cyclic}). \tag{2.39}$$

$$K = \beta(\Sigma \cdot L + 1). \tag{2.40}$$

V is the Coulomb potential and L is the orbital angular momentum.

We write the wave function as [74]

$$\psi^\mu_\kappa = \begin{pmatrix} g_\kappa(r)\chi^\mu_\kappa \\ if_\kappa(r)\chi^\mu_{-\kappa} \end{pmatrix}, \tag{2.41}$$

such that $K\psi^\mu_\kappa = -\kappa\psi^\mu_\kappa$ and $J_3\psi^\mu_\kappa = \mu\psi^\mu_\kappa$, where J_3 is the third component of the total angular momentum $\vec{J}$. The radial functions g_κ and f_κ obey the differential equations

$$\frac{dg_\kappa(r)}{dr} = -\frac{\kappa+1}{r}g_\kappa(r) + (E - V + 1)f_\kappa(r), \tag{2.42}$$

$$\frac{df_\kappa(r)}{dr} = \frac{\kappa-1}{r}f_\kappa(r) - (E - V - 1)g_\kappa(r). \tag{2.43}$$

In the high energy limit -all the masses are set to zero- and from eqs.(2.42) and (2.43), $f_\kappa(r)$ and $g_\kappa(r)$ satisfy

$$f_{-\kappa} = -g_\kappa, \qquad g_{-\kappa} = f_\kappa. \tag{2.44}$$

From here on we make use of this result for the spinor $\psi^{\mu(e)}_{\kappa,E}$ describing the electrons coming from the conversion process. The initial muon instead is described by ψ^{μ}_{κ} with the quantum numbers, $\mu = \pm\frac{1}{2}$ and $\kappa = -1$ and we choose the normalization

$$\int d^3x \psi^{(\mu)\dagger}_{1s}(\vec{x})\psi^{(\mu)}_{1s}(\vec{x}) = 1. \tag{2.45}$$

For the electrons in the continuum-energy states we use the same normalization considered in [72], namely

$$\int d^3x \psi^{\mu(e)\dagger}_{\kappa,E}(\vec{x})\psi^{\mu^{'}(e)}_{\kappa^{'},E^{'}}(\vec{x}) = 2\pi\delta_{\mu\mu^{'}}\delta_{\kappa^{'}\kappa}\delta(E - E^{'}). \tag{2.46}$$

In the conversion process the effective Hamiltonian is given by [72]

$$\begin{aligned} H_{eff} &= \frac{4G_F}{\sqrt{2}}(m_\mu A^*_R \bar{\mu}\sigma^{\mu\nu}P_L e F_{\mu\nu} + m_\mu A^*_L \bar{\mu}\sigma^{\mu\nu}P_R e F_{\mu\nu} + h.c.) \\ &+ \frac{G_F}{\sqrt{2}}\sum_{q=u,d,s}[(g_{LS(q)}\bar{e}P_R\mu + g_{RS(q)}\bar{e}P_L\mu)\bar{q}q + (g_{LP(q)}\bar{e}P_R\mu + g_{RP(q)}\bar{e}P_L\mu)\bar{q}\gamma_5 q \\ &(g_{LV(q)}\bar{e}\gamma^\mu P_L\mu + g_{RV(q)}\bar{e}\gamma^\mu P_R\mu)\bar{q}\gamma_\mu q + (g_{LA(q)}\bar{e}\gamma^\mu P_L\mu + g_{RA(q)}\bar{e}\gamma^\mu P_R\mu)\bar{q}\gamma_\mu\gamma_5 q + \\ &\frac{1}{2}(g_{LT(q)}\bar{e}\sigma^{\mu\nu}P_R\mu + g_{RT(q)}\bar{e}\sigma^{\mu\nu}P_L\mu)\bar{q}\sigma_{\mu\nu}q + h.c.]. \end{aligned} \tag{2.47}$$

The nuclear form factors were calculated in [75]. The wave function for the muon and the electrons in the presence of a central field were obtained in [71, 72]. In particular in [72] updated data for the proton and neutron densities were used.

In the limit of $r \to \infty$ it can be shown that the general solution for a Dirac particle in a Coulomb field at first order in H_{eff} is of the form [73]

$$\psi_{as} = -i\sqrt{\frac{\pi}{|\vec{p}|}}\frac{e^{ipr}}{r}\sum_{\kappa\mu} e^{i\delta_\kappa}\langle\psi_\kappa^{(e)\mu}|H_{eff}|\psi_{1s}^{(\mu)}\rangle \begin{pmatrix} \sqrt{E+1}\chi_\kappa^\mu(\hat{p}) \\ -\sqrt{E-1}\chi_{-\kappa}^\mu(\hat{p}) \end{pmatrix} + \mathcal{O}(H_{eff}^2), \tag{2.48}$$

where $\hat{p}$ is in the direction of the outgoing electron. The phases $e^{i\delta_\kappa}$ are the usual ones appearing in scattering problems in the presence of a Coulomb field and are given by

$$\delta_\kappa = y\ln 2pr - \arg\Gamma(\gamma + iy) + \eta_\kappa - \frac{1}{2}\pi\gamma, \tag{2.49}$$

$$y = \alpha ZE/p, \quad \gamma = \sqrt{\kappa^2 - \alpha^2 Z^2}, \quad e^{2i\eta_\kappa} = -\frac{\kappa - iy/E}{\gamma + iy} \tag{2.50}$$

where Z is the atomic number, $\alpha = e^2/4\pi$ and p is the modulus of the 3-momentum $\vec{p}$. We consider states with $\kappa = \pm 1$, hence the only term relevant for our discussion is η_κ –the remaining ones are just an overall phase in the solution ψ_{as}.

Finally the total conversion rate per unit flux is

$$\omega_{conv} = R^2\int d\Omega\psi_{as}^\dagger\psi_{as} = \frac{1}{2}\sum_{\kappa,\mu}|\langle\psi_\kappa^\mu|H_{eff}|\psi_i\rangle|^2. \tag{2.51}$$

In the next section we discuss the total conversion rate in some detail.

2.4.3 Total conversion rate

In this section we briefly comment about the amplitude of the $\mu \to e$ conversion process and the Born's approximation we used.

In computing the $\mu \to e$ conversion process, one usually assumes the so called Born's approximation for the outgoing electrons. This approximation has two meanings: one is computing the conversion rate to a given order in some small coupling; and the other is the assumption that electrons coming from the conversion process are plane waves. The point is that we can do better and have a complete control of both approximations at the same time. More precisely for the relativistic one-electron atom and in the limit of big r ($r >> r_0$, where $V(r \geq r_0) = 0$), the solution of the

Dirac's equation at first order in the perturbation H_{eff} is of the form [73]

$$\psi_{as} = -i\sqrt{\frac{\pi}{|\vec{p}|}}\frac{e^{ipr}}{r}\sum_{\kappa\mu} e^{i\delta_\kappa}\langle\psi^\mu_\kappa|H_{eff}|\psi_i\rangle \begin{pmatrix} \sqrt{E+1}\chi^\mu_\kappa(\hat{p}) \\ -\sqrt{E-1}\chi^\mu_{-\kappa}(\hat{p}) \end{pmatrix} + \mathcal{O}(H^2_{eff}), \tag{2.52}$$

where ψ_i is any stationary state of the Coulomb potential, ψ^μ_κ is one of the continuum energy solutions and H_{eff} is the effective Hamiltonian for the $\mu \to e$ conversion process. Furthermore it can be shown that ψ_{as} is an eigenfunction of $\vec{\alpha}\cdot\vec{p}+\beta$ with eigenvalue E so that ψ_{as} describes, indeed a plane wave [73]. In the high energy limit –neglecting the electron mass– the solution ψ_{as} simplifies to

$$\psi_{as} = -i\sqrt{\pi}\frac{e^{ipr}}{r}\sum_{\kappa\mu} e^{i\delta_\kappa}\langle\psi^\mu_\kappa|H_{eff}|\psi_i\rangle \begin{pmatrix} \chi^\mu_\kappa(\hat{p}) \\ -\chi^\mu_{-\kappa}(\hat{p}) \end{pmatrix}. \tag{2.53}$$

Finally if we are interested in computing the total conversion amplitude per unit flux (for a detector placed at fixed radius $r = R$) the total conversion rate is given by

$$\omega_{conv} = R^2\int d\Omega\psi^\dagger_{as}\psi_{as} = 2\pi\left(\frac{1}{2}\sum_{\kappa,\mu}|\langle\psi^\mu_\kappa|H_{eff}|\psi_i\rangle|^2\right) \tag{2.54}$$

and we may absorb the $\sqrt{2\pi}$ factor into the normalization of the wave function ψ^μ_κ in order to agree with the conventions adopted in [72].

2.4.4 Triple vector correlation in the conversion process

In this section we give details of the calculation for the triplet correlation asymmetry in the $\mu \to e$ conversion process within the formalism developed in [73]. We make use of the formalism to compute the triple vector correlations shown in chapter 4.

Since we are interested in describing particles with a given polarization, we are going to make use of the spin projection operators for Dirac spinors. Instead of using the covariant spin projection operator we make use of the following projection operator

$$P^{(\pm)}_{\hat{n}_0} = \frac{1}{2}(1 \pm \mathcal{O}\cdot\hat{n}_0), \tag{2.55}$$

where

$$\mathcal{O} \equiv \beta\vec{\sigma} + (1-\beta)(\vec{\sigma}\cdot\hat{p})\hat{p} \tag{2.56}$$

and $\hat{n_0}$ is the direction of the spin polarization vector in the rest frame of the particle, $\hat{p}$ is the direction of its momentum and the $\pm$ represent positive and negative polarization respectively. It can be shown that the description of the spin with this operator is equivalent to the usual one given by the manifestly covariant spin operator [4] . Notice that the non-relativistic limit of can be taken in a transparent way by replacing $\beta \to 1$.

For our present problem we assumed the muon to be non-relativistic and in the frame shown in Fig.2.1 its polarization vector is of the form

$$n_\mu = (0, \hat{n}_0), \tag{2.57}$$

where

$$\hat{n}_0 = (\sin\Phi\cos\Psi, \sin\Phi\sin\Psi, \cos\Phi). \tag{2.58}$$

By multiplying the wave function of the muon in the conversion process by $P^{(+)}_{\hat{n}_0}$ one obtains the wave function of a non-relativistic muon with the given polarization. For the electron instead a full relativistic treatment is required since its energy is $E_e = m_\mu - \epsilon_b$, where m_μ is the muon mass and ϵ_b is the binding energy of the muon in the 1s state of the muonic atom. In this case the spin projection operator coming from the conversion process is given by

$$P^{(+)}_e = \frac{1}{2}(1 + \mathcal{O}^e \cdot \hat{n}^e_0) \tag{2.59}$$

and

$$\mathcal{O}^e \cdot \hat{n}^e_0 = \beta\vec{\sigma}\cdot\hat{n}^e_0 + (1-\beta)(\vec{\sigma}\cdot\hat{p}_e)(\hat{p}_e\cdot\hat{n}^e_0), \tag{2.60}$$

$$\hat{n}^e_0 = (0,1,0), \quad \hat{p}_e = (\sin\theta_s, \cos\theta_s, 0). \tag{2.61}$$

[4] see [74] chapter III.

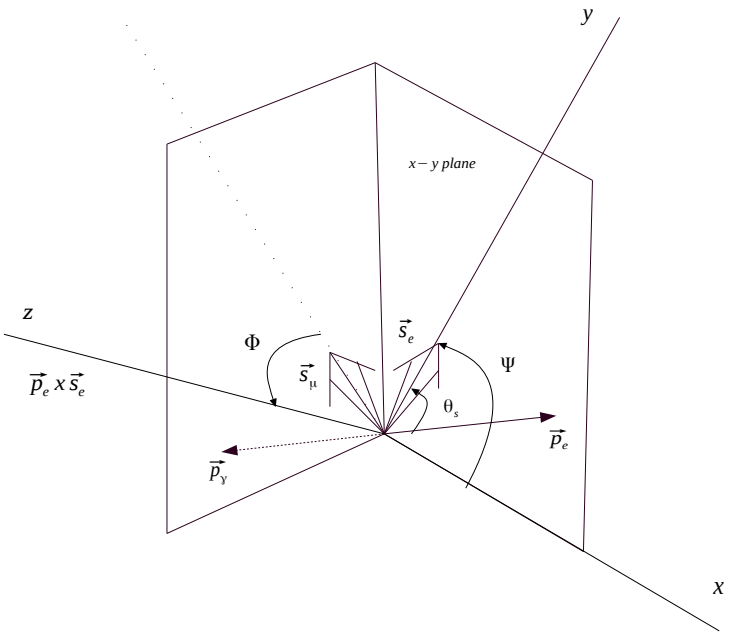

Figure 2.1: Reference frame and the setup for the $\mu \to e\gamma$ decay and the $\mu \to e$ conversion process.

Finally the wave function describing the polarized outgoing electron –coming from the conversion of a polarized muon– is obtained by applying $P_e^{(+)}$ to the solution (2.48) and then (again for a detector placed at a fixed radius R):

$$\omega_{\text{conv}}(\cos\Phi > 0) - \omega_{\text{conv}}(\cos\Phi < 0) = R^2 \int d\Omega \cdot \text{sgn}(\hat{s}_\mu \cdot (\hat{p}_e \times \hat{s}_e)) \cdot \psi_{as}^\dagger P_e^{(+)} \psi_{as}. \tag{2.62}$$

Which is the expression we use when computing the asymmetry in the conversion process.

Chapter 3

Right-handed lepton mixings at the LHC

In this section we focus on the determination of the elements of the leptonic mixing matrix V_R and propose an strategy to determine its elements at the LHC. In particular the proposed strategy make use of the KS process and the decays of the doubly-charged scalar δ_R^{++} belonging to the $SU(2)_R$ triplet, that as we shall see allow the complete determination of the mixing angles and three CP phases. We also point out that these two processes are not sensitive to three of the phases appearing in V_R, unlike electric dipole moments of charged leptons.

3.1 Determination of the right-handed leptonic mixing matrix

In this section we show how the three angles θ_{12},θ_{23},θ_{13} and the Dirac phase δ, appearing in V_R are all expressed in term of physical observables at the LHC. Furthermore, we find analytic expressions relating the elements of $\hat{V}_R$ with some physical branching ratios of the KS process. For the Majorana phases we point out that they can be obtained through the decays of the doubly charged scalar. Moreover these measurements could serve as a cross-checking for the model. Previous LHC Studies have been done for this process assuming one and two heavy neutrino exchange [76], instead here we do it in the generic case without further assumptions. As we will see our approach has the advantage that the hadronic correction cancel redering the determination of the mixing cleaner too. The determination of the Dirac and some of Majorana phases is in principle possible. Finally another obvious advantage is that this approach allow the immediate implementation and testing in Monte Carlo generators such as MadGraph [77] and Pythia [78].

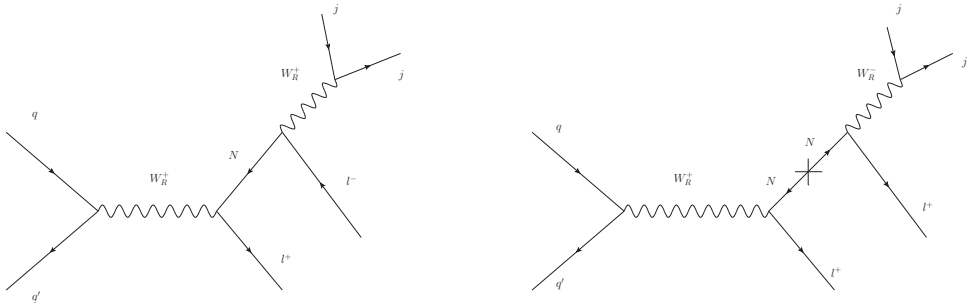

Figure 3.1: Keung-Senjanović process in both opposite-sign leptons (Left) and the lepton-number-violating same-sign leptons in the final state (Right).

3.1.1 Keung-Senjanović process

We begin our analysis by considering the KS process. It has a clean LNV channel that consists in two same-sign leptons and two jets in the final state with almost no background. This process has no missing energy in the final state and it is amplified by the W_R resonance. Measuring the energy and momenta of the final particles it allows the full reconstruction of the masses of the W_R and the heavy neutrino N. Studies of this process were performed in the past [79, 80, 81, 82, 83], with the conclusion that W_R can be discovered at the LHC with a mass up to $\simeq 6$ TeV, masses for the right-handed neutrinos of the order $m_N \simeq 100$GeV- 1TeV for 300 fb^{-1} of integrated luminosity. In [84, 85] completed studies of the W_R production and decays at the LHC were done. They gave special emphasis to the chiral couplings of the W_R with initial and final state quarks as well as the final state leptons. They showed that it is possible to determine (by studying angular correlations and asymmetries between the participating particles) the chiral properties of W_R and the fermions.

The KS process offers also the possibility of observing both the restoration of the Left-Right symmetry and the Majorana nature of neutrinos at colliders (see FIG. 3.1). The latter implies the equality between the decay rates in the same-sign and the opposite-sign leptons in the final state [16].

Once W_R is produced on-shell, it decays into a lepton and the heavy neutrino N. For W_R boson mass bigger than the masses of the heavy neutrinos N_α (namely, $m_N < m_{W_R}$) where $\alpha =$

$1, 2, 3$, the decay rate of $W_R \to l_i l_k jj$ is (no summation over repeated indices)

$$\Gamma(W_R^+ \to l_i^+ l_k^+ jj) = \sum_{qq'} \Gamma(W_R^+ \to l_i^+ l_k^+ qq^{'}) = \sum_{qq'} \Gamma(W_R^+ \to l_i^+ N_\alpha)\mathrm{Br}(N_\alpha \to l_k^+ qq^{'}), \tag{3.1}$$

where $i, k = e, \mu, \tau$ and "Br" denotes the branching ratio into a given channel. A comment here is in order, we assume that the electron produced together with W_R may be distinguished from the electron coming from the decay of the heavy neutrino N. For instance, in [79, 85] it is shown that this distinction may be done using the appropriate kinematical variable. More precisely in [79] they assumed that the electron with the lowest value of the quantity $m_N^{\mathrm{rec}} - m_{\mathrm{inv}}(ejj)$ comes from the decay of the heavy neutrino, where m_N^{rec} and $m_{\mathrm{inv}}(ejj)$ are the reconstructed mass of the heavy neutrino and the invariant mass of the ejj system respectively. This distinction turns out to be crucial for it allows to measure the polarization effects of the leptonic decays of the W_R boson. Notice that when the heavy neutrino N decays through m_D or into left-handed charged leptons [6] and/or in the form of displaced vertex at the LHC [81] the distinction becomes more apparent. In the case when the two leptons are indistinguishable, there is another diagram that contributes in the amplitude giving a net factor of two in the probability –since the phase space is reduced by a factor of two as well. Conversely for two different leptons there is a factor of two in the probability since both contributions sum up incoherently. The bottom line is that amount to adding a term in Eq. 3.1 with $i \leftrightarrow k$. On the other hand, since we shall consider ratios of cross sections, our results are unaffected.

In the case of on-shell W_R and N eq. (3.1) will not be modified by hadronic corrections between initial and final quarks and the argument goes as follows: since this diagram can be interpreted as a process occurring in space-time [86] , it is clear that there will be no interference between the tree level process and the loop-corrections joining the initial and final quark states since in the loop corrections W_R and N are off-shell particles. In the case of an off-shell, KS-process loop corrections between initial and final quarks may play an important role but this is not the case we are considering, adding the fact that this process by itself is not so interesting since there is no an

enhancement in the amplitude due to internal on-shell particles.

Notice that if the heavy neutrino masses are not degenerate, in general the KS process is sensitive only to the Dirac type phase δ. In this case both lepton number conserving and lepton number violating channels give the same results. The partonic processes are illustrated in FIG. 3.1.

For degenerate heavy neutrino masses, namely mass differences less or equal than their total width i.e. $\Delta m_N \leq \Gamma(N)$, one may easily see from the same-sign leptons in the final state, that there is a CP-even dependence on the phases in K_N. Notice that this channel breaks the total lepton number, then is clear that we should have some dependence on the Majorana phases. In the case of at least two degenerate heavy neutrino masses, it is in principle possible to construct CP-odd, triple-vector-product asymmetries with three momenta or any mixture of momenta and spin for the participating particles. For instance in [87] CP odd asymmetries at the LHC are constructed and it is found that there could be significant sensitivity to CP-odd couplings.

From Eq. (2.19) we find that the decay rate of $W_R^+ \to l_i^+ N_\alpha$ is (in the rest frame of the W_R boson)

$$\Gamma(W_R^+ \to l_i^+ N_\alpha) = \frac{g^2}{8\pi}|(V_R^\dagger)_{\alpha i}|^2 \frac{|\vec{p}_2^{\,\alpha}|^2}{m_{W_R}^2}[\frac{|\vec{p}_2^{\,\alpha}|}{3} + E_2^\alpha], \tag{3.2}$$

$\vec{p}_2^{\,\alpha}$ is the momentum of the right-handed neutrino N_α. E_2^α is the energy of N_α and $\vec{p}_2^{\,\alpha}$ is such that

$$|\vec{p}_2^{\,\alpha}| + \sqrt{|\vec{p}_2^{\,\alpha}|^2 + m_{N_\alpha}^2} = m_{W_R}. \tag{3.3}$$

The 3-body decay rate of N into one lepton and two jets is given by

$$\Gamma(N_\alpha \to l_k^+ jj) = N_C \tfrac{g^4}{512\pi^3}|(V_R^\dagger)_{\alpha k}|^2 F(\tfrac{m_N}{m_{W_R}}) m_{W_R} \left(\textstyle\sum_{qq'} |(V_R^Q)^\dagger_{qq'}|^2\right), \tag{3.4}$$

with,

$$F(x) = -\tfrac{1}{2}x(1+\tfrac{x^2}{3}) + x^{-3}\left[(1-x^2)\ln(1-x^2) + x^2\right], \quad x < 1, \tag{3.5}$$

where V_R^Q is the right-handed quark mixing matrix, N_C is the number of colors and the sum over q, q' includes the kinematically allowed heavy neutrino decays. When $x \ll 1$, $F(x) = x^5/12 + \mathcal{O}(x^7)$ and this corresponds to the decay rate in the limit $m_N \ll m_{W_R}$.

For heavy neutrinos masses above the pion threshold, the dominant decay rate are the hadronic ones and the branching ratio into one charged lepton and two jets is given by

$$\mathrm{Br}(N_\alpha \to l_k^+ jj) = \frac{\Gamma(N_\alpha \to l_k^+ jj)}{\Gamma(\sum_k N_\alpha \to l_k^+ jj)} \simeq |(V_R^\dagger)_{\alpha k}|^2 \tag{3.6}$$

and, according to eq. (3.1), the following ratio takes the simple form

$$\frac{\Gamma(W_R^+ \to N_\alpha l_i \to l_i^+ l_k^+ jj)}{\Gamma(W_R^+ \to N_{\alpha'} l_r \to l_r^+ l_s^+ jj)} = \frac{\sigma(pp \to W_R^+ \to N_\alpha l_i \to l_i^+ l_k^+ jj)}{\sigma(pp \to W_R^+ \to N_{\alpha'} l_r \to l_r^+ l_s^+ jj)} = \frac{|(V_R^\dagger)_{\alpha i}|^2 |(V_R^\dagger)_{\alpha k}|^2 c^\alpha}{|(V_R^\dagger)_{\alpha' r}|^2 |(V_R^\dagger)_{\alpha' s}|^2 c^{\alpha'}}, \tag{3.7}$$

where

$$c^\alpha \equiv |\vec{p}_2^{\,\alpha}|^2 [\frac{|\vec{p}_2^{\,\alpha}|}{3} + E_2^\alpha], \tag{3.8}$$

all the hadronic and quark mixing part cancels and we end up having a quantity that depends only on the physical masses and the elements of V_R. When $\alpha = \alpha'$ the expression further simplifies and depends only on the elements of V_R.

In what follows we consider the case when one, two or three heavy neutrinos are accessible at the LHC.

One heavy neutrino case: it may happen that even if the W_R is found at the LHC, just one of the heavy neutrino mass can be reconstructed. In this case we see from Eq. (3.7) (taking $r = s = \mu$) that there are only two independent quantities including tau leptons in the final state, where "independent quantities" refers to the ones that can be measured in the experiment.

If only electrons and muons are considered is easy to see that there is only one independent quantity within this analysis.

Two heavy neutrinos case: one expect for two heavy neutrino at the LHC, that in order to probe all the elements of the mixing matrix V_R the decays of the heavy neutrinos N into electrons, muons and tau leptons must be identified. In fact, in this case analytical solutions for the three mixing angles and the Dirac phase δ can be found in terms of physical quantities at the LHC, this

can be seen by considering $\alpha = \alpha'$ in Eq. (3.7), namely

$$\frac{\Gamma(W_R^+ \to N_\alpha e^+ \to e^+\mu^+ jj)}{\Gamma(W_R^+ \to N_\alpha \mu^+ \to \mu^+\mu^+ jj)} = \frac{|(V_R^\dagger)_{\alpha e}|^2}{|(V_R^\dagger)_{\alpha\mu}|^2} \equiv R_\alpha, \tag{3.9}$$

where

$$\alpha = 1, 2.$$

There are 4 unknown parameters in $\hat{V}_R$ (θ_{12}, θ_{13}, θ_{23} and δ). By using the above ratios it is possible to probe 2 of them. There is just another independent quantity considering electron and muons in the final state

$$\frac{\Gamma(W_R^+ \to N_1 e^+ \to e^+ e^+ jj)}{\Gamma(W_R^+ \to N_2 e^+ \to e^+ e^+ jj)} \equiv R_4 = \frac{|(V_R^\dagger)_{1e}|^4 c^{(1)}}{|(V_R^\dagger)_{2e}|^4 c^{(2)}}. \tag{3.10}$$

So we conclude that in order to probe the three mixings angles and the Dirac phase with 2 heavy neutrinos on-shell, tau leptons must be included into the analysis and to this end consider the following relation

$$\frac{\Gamma(W_R^+ \to N_1 e^+ \to e^+ e^+ jj)}{\Gamma(W_R^+ \to N_1 e^+ \to e^+ \tau^+ jj)} = \frac{|(V_R^\dagger)_{1e}|^2}{|(V_R^\dagger)_{1\tau}|^2} \equiv R_\tau \tag{3.11}$$

and the mixings angles are given by

$$s_{12}^2 = \frac{1}{\sqrt{\frac{c^{(2)}}{c^{(1)}} R_4} + 1}, \quad s_{13}^2 = \frac{-\frac{R_\tau R_1}{\sqrt{\frac{c^{(2)}}{c^{(1)}} R_4}} + R_1 + R_\tau}{R_\tau R_1 + R_1 + R_\tau}, \quad s_{23}^2 = \frac{\left(\frac{1}{R_\tau} + \frac{1}{R_2} + 1\right)\sqrt{\frac{c^{(2)}}{c^{(1)}} R_4}}{\sqrt{\frac{c^{(2)}}{c^{(1)}} R_4} + 1} - \frac{1}{R_2}. \tag{3.12}$$

Perhaps the more important advantage of the above expressions is that they allow a simple interpretation of the three leptonic mixing angles in terms of the final states in the KS process. For instance, from (3.12) we may see that θ_{12} is maximal when $R_4 \ll 1$ and minimal when $R_4 >> 1$. For θ_{13} we notice that its value is maximal whenever $R_1 \ll 1$ or $R_\tau \ll 1$. Instead it is minimal when the relation $R_1 + R_\tau = R_1 R_\tau / \sqrt{\frac{c^{(2)}}{c^{(1)}} R_4}$ is satisfied. Finally θ_{23} takes its maximal value when $R_4 >> 1$ and $R_\tau >> 1$ and its minimal value when $R_4 \ll 1$ and $R_2 >> 1$. For instance in table 3.1, we show the conditions that the final states should satisfy in order to have maximal or minimal mixing angles. More precisely, the θ_{12} mixing angle would be nearly maximal whenever the rate of

Mixing angle	**Maximal mixing**	**Zero mixing**
θ_{12}	$\sigma(pp; N_1 e^{\pm}; e^{\pm} e^{\pm} jj) \ll \sigma(pp; N_2 e^{\pm}; e^{\pm} e^{\pm} jj)$	$\sigma(pp; N_1 e^{\pm}; e^{\pm} e^{\pm} jj) \gg \sigma(pp; N_2 e^{\pm}; e^{\pm} e^{\pm} jj)$
θ_{23}	$\sigma(pp; N_1 e^{\pm}; e^{\pm} e^{\pm} jj) \gg \sigma(pp; N_2 e^{\pm}; e^{\pm} e^{\pm} jj)$ and $\sigma(pp; N_1 e^{\pm}; e^{\pm} e^{\pm} jj) \gg \sigma(pp; N_2 e^{\pm}; e^{\pm} \tau^{\pm} jj)$	$\sigma(pp; N_1 e^{\pm}; e^{\pm} e^{\pm} jj) \ll \sigma(pp; N_2 e^{\pm}; e^{\pm} e^{\pm} jj)$ and $\sigma(pp; N_2 \mu^{\pm}; \mu^{\pm} \mu^{\pm} jj) \ll \sigma(pp; N_2 e^{\pm}; e^{\pm} \mu^{\pm} jj)$
θ_{13}	$\sigma(pp; N_1 \mu^{\pm}; \mu^{\pm} \mu^{\pm} jj) \gg \sigma(pp; N_1 e^{\pm}; e^{\pm} \mu^{\pm} jj)$ or $\sigma(pp; N_1 e^{\pm}; e^{\pm} e^{\pm} jj) \ll \sigma(pp; N_1 e^{\pm}; e^{\pm} \tau^{\pm} jj)$	$\sqrt{\frac{c^{(2)}}{c^{(1)}} R_4} = \frac{R_1 R_\tau}{R_1 + R_\tau}$

Table 3.1: Conditions that the maximal/minimal mixing angles should satisfy in terms of the final states for the KS process for two heavy neutrinos at the LHC.

N_1 with two electrons is suppressed with respect to the rate of N_2 with two electrons, and it would be nearly zero in the opposite case. For the mixing angle θ_{23} we may see that it would be nearly maximal whenever the rate of N_1 with two electrons is enhanced with respect to the rate of N_2 with two electrons and in addition the rate of N_1 with two electrons, is enhanced with respect to the rate of N_2 with one electron and and one tau lepton. Instead it would be nearly zero, if the rate of N_1 with two electrons is suppressed with respect to the rate of N_2 with two electrons, and in addition the rate of N_2 with two muons, is reduced with respect to the rate of N_2 with one electron and one muon. Finally the mixing angle θ_{13} would be maximal if the rate of N_1 with one electron and one muon is suppressed with respect to the mixing of N_1 with two muons, and in addition the rate of N_1 with two electrons is suppressed with respect to the rate of N_1 with one electron and one tau lepton in the final state.

For the sake of simplicity we show the expression for the Dirac phase δ in terms of R_1 and the mixing angles and it is given by

$$\cos\delta = \frac{c_{13}^2 c_{12}^2 - R_1(c_{23}^2 s_{12}^2 + c_{12}^2 s_{13}^2 s_{23}^2)}{2 c_{12} c_{23} s_{12} s_{13} s_{23} R_1}. \tag{3.13}$$

CP-violating phase	Maximal Dirac CPV Conditions
(first case) δ	$\sigma(pp; N_1 e^\pm; e^\pm e^\pm jj) \simeq \sigma(pp; N_2 e^\pm; e^\pm e^\pm jj)$ and $\frac{\sigma(pp; N_1 e^\pm; \mu^\pm e^\pm jj)}{\sigma(pp; N_1 \mu^\pm; \mu^\pm \mu^\pm jj)} \simeq \frac{\sigma(pp; N_2 e^\pm; e^\pm \mu^\pm jj)}{\sigma(pp; N_2 \mu^\pm; \mu^\pm \mu^\pm jj)}$
(second case) δ	$\sigma(pp; N_1 e^\pm; e^\pm \tau^\pm jj) \gg \sigma(pp; N_1 e^\pm; e^\pm e^\pm jj) \simeq \sigma(pp; N_2 e^\pm; e^\pm e^\pm jj)$

Table 3.2: Conditions that lead to the maximal CP violation from the phase δ for the two heavy neutrinos at the LHC.

In the appendix C we show the complete expression for $\cos\delta$ in terms of the physical quantities at the LHC. We found two rather simple limiting cases that would imply the maximal value for the phase δ. Expressed in terms of the final states the first case is when the rate involving N_1 with two electrons in the final state is equal to the rate of the process involving N_2 with two electrons in the final state, together with $\frac{\sigma(pp; N_1 e^\pm; \mu^\pm e^\pm jj)}{\sigma(pp; N_1 \mu^\pm; \mu^\pm \mu^\pm jj)} \simeq \frac{\sigma(pp; N_2 e^\pm; e^\pm \mu^\pm jj)}{\sigma(pp; N_2 \mu^\pm; \mu^\pm \mu^\pm jj)}$. The second limiting case is when the rate for N_1 with one electrons and one tau in the final state is much bigger than the rate involving N_1 with two electrons in the final state, that is equal to the rate of the process involving N_2 with two electrons in the final state. For the sake of clarity in table 3.2 we show the these two conditions explicitly.

In order to see how the above results are affected once hadronization effects are taken into account, we extent the Feynrules implementation of the mLRSM in [88] to include leptonic mixing in the type II see-saw dominance for $\mathcal{C}$ as the LR symmetry, where it can be shown that $V_R = K_e V_L^*$. The events at the parton level are simulated with Madgraph 5 [77] and hadronization effects with Pythia 6 [78]. We use the same cuts applied in [79, 80, 81], namely both jets must have transverse energy grater than 100 GeV and the invariant mass of the two final leptons grater than 200 GeV. We take $\theta_{12} = 35^o$, $\theta_{23} = 45^o$, $\theta_{13} = 7^o$ and $\delta = 0$ in this illustrative example.

Furthermore, there is a proportionality between the two neutrino mass matrices

$$\frac{M_N}{\langle \Delta_R \rangle} = \frac{M_\nu^*}{\langle \Delta_L \rangle^*}, \tag{3.14}$$

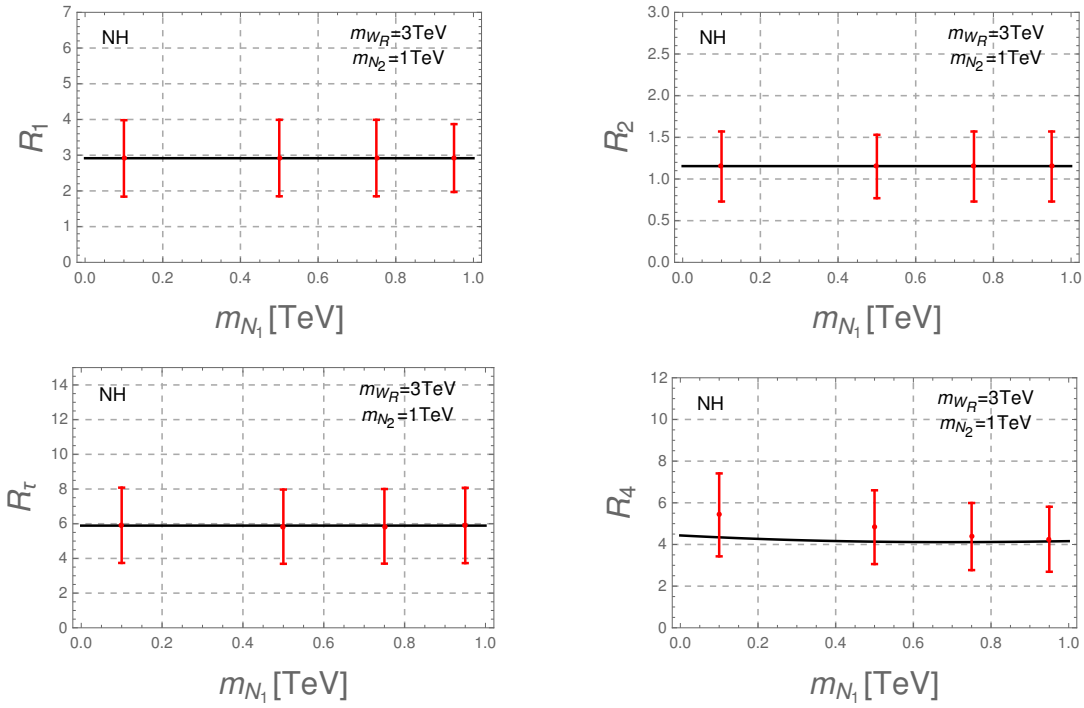

Figure 3.2: Plots for the quantities R_1,R_2,R_τ and R_4 in the type II see-saw dominance ($V_L \propto V_R^*$) as a function of the lightest neutrino mass eigenstate for 2 heavy neutrinos at the LHC in the NH case. Red dots with errors bars are the results obtained by taking into account the hadronization effects using Pythia 6. We assume the values of the gauge boson $m_{W_R} = 3$ TeV and the heavy neutrino mass $m_{N_2} = 1$ TeV

which implies [89, 90]

$$\frac{m_{N_2}^2 - m_{N_1}^2}{m_{N_3}^2 - m_{N_1}^2} = \frac{m_{\nu_2}^2 - m_{\nu_1}^2}{m_{\nu_3}^2 - m_{\nu_1}^2} \simeq \pm 0.03, \tag{3.15}$$

where the $\pm$ corresponds to normal/inverted (NH/IH) neutrino mass hierarchy respectively. Notice that once the Left-Right symmetry is discovered, this possibility can be verify or falsify by the experiments. We show in Fig. 3.2 in the case of normal hierarchy neutrino mass spectrum and for heavy neutrino masses accessible at the LHC, the results obtained from the simulation, where it can be readily seen that our suggested strategy for measuring the right handed mixing angles is feasible at hadron colliders such as the LHC and future ones. Notice that for the IH case, neutrino mass spectra accessible at the LHC would imply that only one or three neutrino masses can be reconstructed. The largest uncertainties in the production cross sections arises from the uncertainties in the parton distribution functions PDF's of the proton and we assume them to be 26% for $m_{W_R} = 3$ TeV as reported in [43] for 7 TeV of the center of mass energy. Although in this work we consider 13 TeV of center of mass energy, one does not expect this result to change considerably. The assumed theoretical uncertainties of the PDF's imply that the mixing angles $\{\theta_{12}, \theta_{23}, \theta_{13}\}$ may determined with 10%, 20% and 66% accuracy respectively for the values of the mixing angles shown and summing the uncertainties in quadrature. Of course this uncertainties may be diminished in the future and become less important at higher energies as the perturbative QCD computations become more reliable. All this assuming 100% identification of the tau leptons in the final state. This issue and the expected sensitivity to the leptonic mixing angles, CP phases is left for future work.

Reconstruction at the detector level becomes more delicate since for low values of the ratio $r = m_N/m_{W_R} \lesssim 0.1$, the decay products of the heavy neutrinos are difficult to separate in the detector, so one would be tempted to conclude that no flavor tagging may be done in this case. This issue was already studied in detail in [79], where it is claimed that for low values of r, one should search for final states with one high p_T isolated lepton and one high p_T jet with large electromagnetic component and matching the high-p_T track in the inner detector for electrons and in the magnetic

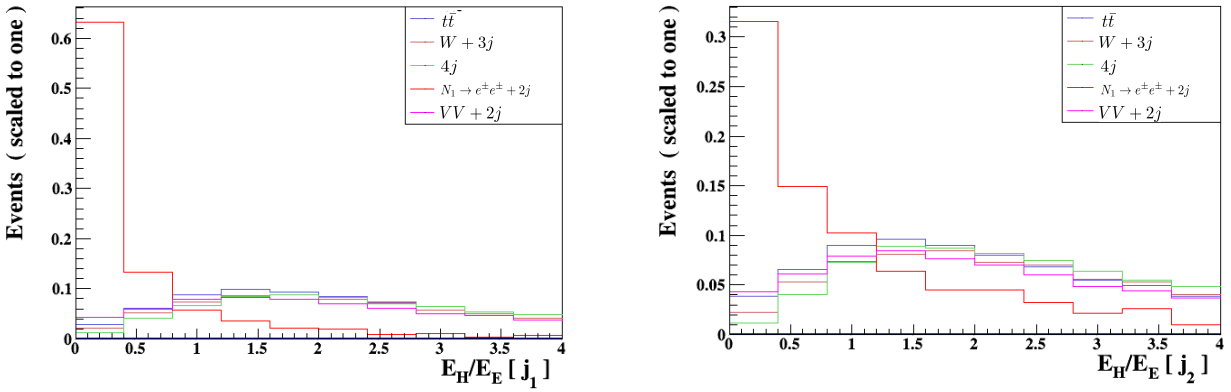

Figure 3.3: Number of events (scaled to one) as a function of the ratio E_H/E_E between the Hadronic energy E_H and the electromagnetic energy E_E for the two hardest jets in energy ($E(j_1) > E(j_2)$) coming from the process $p + p \to W_R^\pm \to N_1 e^\pm \to e^\pm e^\pm + jj$ together with the main SM backgrounds. We assume $m_{W_R} = 3$ TeV and $m_{N_1} = 100$ GeV, $m_{N_2} = 2$ TeV and $m_{N_3} = 2$ TeV. The generic label V stands for the gauge bosons W or Z.

spectrometer for muons. For instance they found out that for $r = 0.1$ the efficiency is lowered to around 46% [79].

Notice that in the particular example we are considering r could be as low as $r \simeq 0.03$, so that one would expect the efficiency to be lower in this case. In order to assess the efficiency we use the Delphes [91] for detector simulation (with the default updated Delphes card for the ATLAS detector) and Madanalysis 5 for event counting and cuts [92]. As in [79] we select the events with one isolated electron (or muon) with $\Delta R > 0.5$ and one isolated jet requiring their transverse energies bigger than 1 TeV, with $\Delta R = \sqrt{\Delta\eta^2 + \Delta\phi^2}$ where η and ϕ are the pseudo-rapidity and the azimuthal angle respectively. We find that the efficiency gets as low as 35% for one high-p_T electron and one high-p_T jet in the final state and as low as 28% for one high p_T muon and high-p_T jet in the final state. Therefore this rises the required luminosity from 64 fb^{-1} to 446 fb^{-1} for the two heavy neutrino case at LHC in the range of masses considered. In estimating the required luminosity we assume the identification efficiency for tau leptons around 50 % in accordance with the efficiencies presented in [93] for the $Z' \to \tau^+\tau^-$ BSM process. For the sake of completeness, in FIG. 3.3 we show the number of events (scaled to one) as a function of the ratio of the energy E_H deposited in the hadronic

calorimeter and the energy E_E deposited in the electromagnetic calorimeter for the two hardest jets in energy (i.e.$E(j_1) > E(j_2)$) coming from the process $p + p \to W_R^{\pm} \to N_1 e^{\pm} \to e^{\pm} e^{\pm} + jj$. As can be seen from the figure the energy deposited in the hadronic calorimeter is much smaller for the signal than for the SM background processes, so in principle one can use this quantity as a discriminating variable between the signal and the backgrounds – as already done in [79].

From table D.1 in appendix A, we see that the smallest cross sections are the ones of the processes involving two muons in the final state with N_1 as intermediate state. We determine the required value for the luminosity by requiring at least 10 events, since a ratio of the signal over the background equal to five is reach much faster due to the LNV character of the final states.

Three heavy neutrinos case: once again in this case it is possible to find analytic expressions for the parameters in V_R in terms of the physical quantities defined in Eq. (3.7). The novelty is that no tau leptons need to be identified in the final state, hence rendering this scenario ideal for the LHC; to this end consider Eqns. (3.9), (3.10) and

$$\frac{\Gamma(W_R^+ \to N_3 e^+ \to e^+ \mu^+ jj)}{\Gamma(W_R^+ \to N_3 \mu^+ \to \mu^+ \mu^+ jj)} = \frac{|(V_R^\dagger)_{3e}|^2}{|(V_R^\dagger)_{3\mu}|^2} \equiv R_3. \tag{3.16}$$

A straightforward computation gives

$$s_{12}^2 = \frac{1}{1 + \sqrt{\frac{c^{(2)}}{c^{(1)}} R_4}}, \quad s_{23}^2 = \frac{R-1}{R_3 - 1}, \quad s_{13}^2 = \frac{R-1}{R - \frac{1}{R_3}}, \tag{3.17}$$

where

$$R \equiv \frac{1}{\sqrt{\frac{c^{(2)}}{c^{(1)}} R_4} + 1} \left[\frac{\sqrt{\frac{c^{(2)}}{c^{(1)}} R_4}}{R_1} + \frac{1}{R_2}. \right] \tag{3.18}$$

One striking feature of the above expressions is that both θ_{13} and θ_{23} are near zero whenever R is close to one, and this in turn implies that R_1 is must be close to R_2. Furthermore θ_{23} is nearly maximal when $R_3 \approx R$ and this relation precisely corresponds to the maximal value θ_{13} when $R_3 \approx R$ but its values are close to one. In table 3.3 we show these same conditions in terms of the final states. In this case θ_{23} and θ_{13} would be close to their minimal value for

Mixing angle	**Maximal mixing**	**Zero mixing**
θ_{12}	$\sigma(pp; N_1 e^\pm; e^\pm e^\pm jj) \ll \sigma(pp; N_2 e^\pm; e^\pm e^\pm jj)$	$\sigma(pp; N_1 e^\pm; e^\pm e^\pm jj) \gg \sigma(pp; N_2 e^\pm; e^\pm e^\pm jj)$
θ_{23}	$R_3 \simeq R$	$\frac{\sigma(pp;N_1 e^\pm;\mu^\pm e^\pm jj)}{\sigma(pp;N_1\mu^\pm;\mu^\pm\mu^\pm jj)} \simeq \frac{\sigma(pp;N_2 e^\pm;e^\pm\mu^\pm jj)}{\sigma(pp;N_2\mu^\pm;\mu^\pm\mu^\pm jj)}$
θ_{13}	$\sigma(pp; N_3 e^\pm; e^\pm\mu^\pm jj) \simeq \sigma(pp; N_3\mu^\pm; \mu^\pm\mu^\pm jj)$	$\frac{\sigma(pp;N_1 e^\pm;\mu^\pm e^\pm jj)}{\sigma(pp;N_1\mu^\pm;\mu^\pm\mu^\pm jj)} \simeq \frac{\sigma(pp;N_2 e^\pm;e^\pm\mu^\pm jj)}{\sigma(pp;N_2\mu^\pm;\mu^\pm\mu^\pm jj)}$

Table 3.3: Conditions that the maximal/minimal mixing angles should satisfy in terms of the final states for the KS process for three heavy neutrinos at the LHC.

$\frac{\sigma(pp;N_1 e^\pm;\mu^\pm e^\pm jj)}{\sigma(pp;N_1\mu^\pm;\mu^\pm\mu^\pm jj)} \simeq \frac{\sigma(pp;N_2 e^\pm;e^\pm\mu^\pm jj)}{\sigma(pp;N_2\mu^\pm;\mu^\pm\mu^\pm jj)}$ as can be readily seen by simple inspection of Eq. 3.17. Finally θ_{13} would be maximal for $\sigma(pp; N_3 e^\pm; e^\pm\mu^\pm jj) \simeq \sigma(pp; N_3\mu^\pm; \mu^\pm\mu^\pm jj)$.

In appendix C we show the expression for Eq. 3.13 in the three NH case as well as the conditions that lead to maximal CP violation due to the phase δ. In this case it is also possible to find simple conditions that lead to the maximal value of $|\cos\delta|$ as explicitly shown in table 3.4. Notice that all the cases that lead to maximal CP violation from the δ phase have the common condition $\frac{c^{(2)}}{c^{(1)}} R_4 \to 1$ for both two and three heavy neutrinos cases.

As it is clear from the above expressions, the elements of $\hat{V}_R$ have in this parametrization simple relations in terms of physical observables at the LHC. The precise form of the Dirac phase δ is shown in (3.13). Notice that for non-degenerate heavy neutrino masses and within this approach one cannot distinguish δ from $-\delta$. In this respect we notice the CP-odd, triple-vector-product asymmetries in $\mu \to e\gamma$ decay and $\mu \to e$ conversion in Nuclei presented in the next sections may resolve this ambiguity and could even discriminate in the most interesting portion of the parameter's space, between $\mathcal{C}$ or $\mathcal{P}$ as the Left-Right symmetry.

CP-violating phase	Maximal Dirac CPV Conditions
(first case) δ	$\sigma(pp; N_1 e^\pm; e^\pm e^\pm jj) \simeq \sigma(pp; N_2 e^\pm; e^\pm e^\pm jj)$ and $\frac{\sigma(pp; N_1 e^\pm; \mu^\pm e^\pm jj)}{\sigma(pp; N_1 \mu^\pm; \mu^\pm \mu^\pm jj)} \simeq \frac{\sigma(pp; N_2 e^\pm; e^\pm \mu^\pm jj)}{\sigma(pp; N_2 \mu^\pm; \mu^\pm \mu^\pm jj)}$
(second case) δ	$\sigma(pp; N_1 e^\pm; e^\pm e^\pm jj) \simeq \sigma(pp; N_2 e^\pm; e^\pm e^\pm jj)$ and $\sigma(pp; N_3 e^\pm; e^\pm \mu^\pm jj) \simeq \sigma(pp; N_3 \mu^\pm; \mu^\pm \mu^\pm jj)$
(third case) δ	$\sigma(pp; N_1 e^\pm; e^\pm e^\pm jj) \simeq \sigma(pp; N_2 e^\pm; e^\pm e^\pm jj)$ and $\sigma(pp; N_2 e^\pm; e^\pm \mu^\pm jj) \ll \sigma(pp; N_2 \mu^\pm; \mu^\pm \mu^\pm jj)$

Table 3.4: Conditions that lead to the maximal CP violation from the phase δ for the three heavy neutrinos at the LHC.

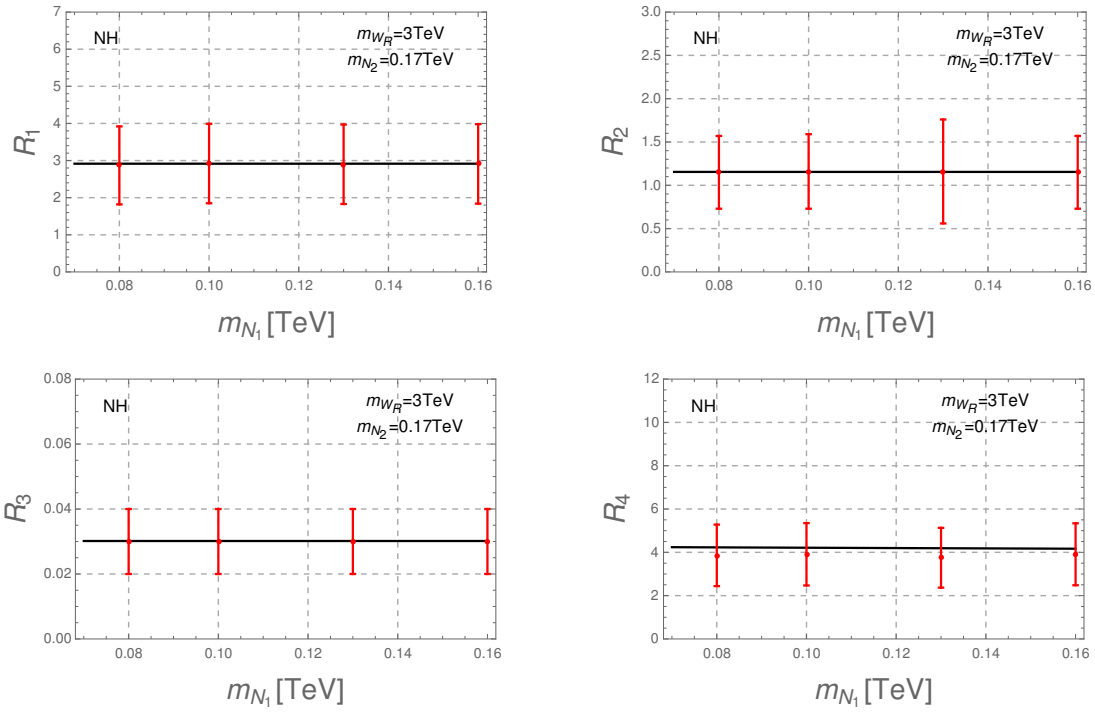

Figure 3.4: Plots for the quantities R_1,R_2,R_3 and R_4 in the type II see-saw dominance ($V_L \propto V_R^*$) as a function of the lightest neutrino mass eigenstate for 3 heavy neutrinos at the LHC in the NH case. Red dots with errors bars are the results obtained by taking into account the hadronization effects using Pythia 6. We assume the values of the gauge boson $m_{W_R} = 3$ TeV and the heavy neutrino mass $m_{N_2} = 0.17$ TeV

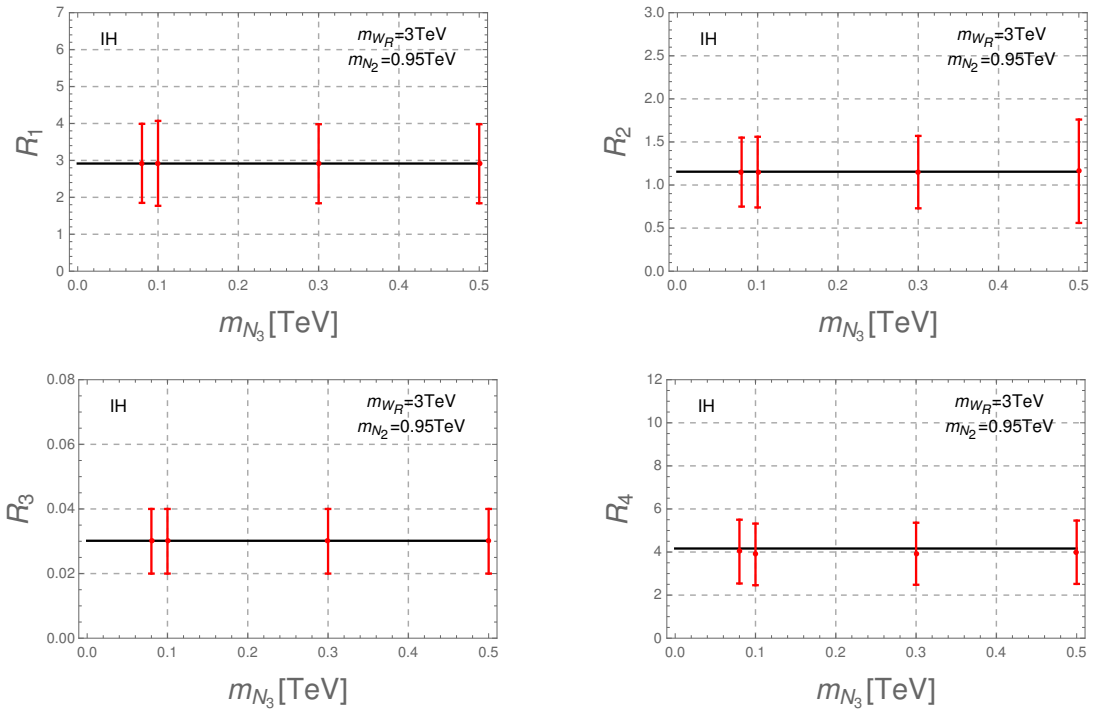

Figure 3.5: Plots for the quantities R_1,R_2,R_3 and R_4 in the type II see-saw dominance ($V_L \propto V_R^*$) as a function of the lightest neutrino mass eigenstate for 3 heavy neutrinos at the LHC in the IH case. Red dots with errors bars are the results obtained by taking into account the hadronization effects using Pythia 6. We assume the values of the gauge boson $m_{W_R} = 3$ TeV and the heavy neutrino mass $m_{N_2} = 0.95$ TeV

In Figs. 3.4 and 3.5 we show the theoretical values for the quantities defined above as well as the result obtained using Madgraph 5 and Pythia 6 indicated by the red dots with their respective error bars. We do it for both normal and inverted neutrino mass hierarchies using Eq. (3.15) for the heavy neutrino masses not listed in the plots. It is clear from the figures that the hadronic corrections to these quantities are under control and assumed to be 26% as in [43], from which we find that the mixing angles $\{\theta_{12}, \theta_{23}, \theta_{13}\}$ may be determined with 10%, 18% and 25% accuracy respectively for the particular values of the mixing angles assumed in this example. We see that despite the value for the mixing angle θ_{13} we used is rather small, it may be determined at the LHC given the present theoretical uncertainties of the PDF's. Future improvements of the perturbative QCD calculations and higher energies may improve the sensitivity.

In this case and from tables D.2 and D.3 in appendix D, we find that for the range of heavy neutrino masses considered i.e. heavy neutrino masses near or bellow the TeV range, the required luminosity necessary for the determination of the three mixing angles is 417 fb^{-1} and 385 fb^{-1} for the NH and IH cases respectively. The required luminosities rise to 1190 fb^{-1} and 1100 fb^{-1} respectively, when detector simulation is included and with the selection criteria explained in the last section. Notice that in this case the required luminosity is bigger than the one for the 2 heavy neutrinos case and this is due to the fact that the mixing of N_3 with the electrons is essentially θ_{13}. Once again and in analogy with the two heavy neutrinos case, we find this value for the luminosity by requiring at least 10 events in the final state, since the ratio of the signal over the background equal to five is reach much faster due to the LNV character of the final states.

3.1.2 Yukawa couplings of the triplet scalars in the LR model

In this section we elaborate in some detail the relation 2.26 previously shown. Notice that the left and right Yukawa couplings of the charged leptons with the doubly charged scalars –in the mass eigenstates basis– are related by

$$Y'_{\Delta_L} = U^* Y'_{\Delta_R} U^\dagger, \tag{3.19}$$

where the precise expression for Y'_{Δ_R} is given in Eq. 2.24 and the matrix U that relates them is given by

$$U \equiv U_{lL}^{\dagger} U_{lR}. \tag{3.20}$$

The matrix U is defined in complete analogy with the matrices U_u and U_d defined in [17, 38, 15], so one can trivially infer what its form must be. Notice that the present case is simpler than the situation in the quark sector studied in [17, 38, 15] since only one matrix U relates the Left and Right Yukawa couplings and its precise form is given by

$$U = \frac{1}{m_l}\sqrt{m_l^2 - it_{2\beta}s_{\alpha}m_l\left[M'_D - t_{\beta}m_l e^{-i\alpha}\right]}, \tag{3.21}$$

so as far as the elements of $M'_D \lesssim m_l$, the factor proportional to $t_{2\beta}s_{\alpha}$ can be treated perturbatively. Following the perturbative computation for the square root of a matrix presented in [15], one finds to the first order in $t_{\beta}s_{\alpha}$ that the elements of U are of the form

$$U_{ij} = (S_l)_{ij} - it_{2\beta}s_{\alpha}R_{ij}, \tag{3.22}$$

with

$$(R)_{ij} = \frac{(M'_D)_{ij}}{(m_l)_i + (m_l)_j} - \frac{1}{2}\tan\beta e^{-i\alpha}(S_l)_{ij}. \tag{3.23}$$

From which Eq. 2.26 readily follows whose precise form is given by

$$Y'_{\Delta_L} = S_l Y'_{\Delta_R} S_l + i\tan\beta\sin\alpha(R^* Y'_{\Delta_R} S_l + S_l Y'_{\Delta_R} R^{\dagger}) + \mathcal{O}\left[(\tan\beta\sin\alpha)^2\right]. \tag{3.24}$$

Notice that this relation does not hold for the Yukawa couplings between the chargeless and singly charged scalars with leptons. The reason is that for the singly charged scalars only δ_L^+ is a physical particle, since its right handed partner δ_R^+ is approximately the would be Nambu-Goldstone boson that becomes the longitudinal component of the gauge boson W_R^+. Instead for the zero-charge scalars δ_L^0 and δ_R^0, there is no relation between the left and right Yukawa couplings with the neutrinos, since the strength of the left and right interactions is proportional to the heavy and light neutrinos masses respectively. These mass matrices are not at all related in the most general case, being the type II see-saw dominance the only exception.

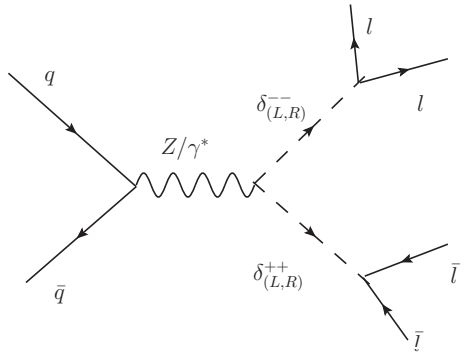

Figure 3.6: Pair production of the doubly charged scalars with Z/γ^* as intermediate states.

3.1.3 Decays of the doubly-charged scalar δ_R^{++}

In the minimal Left-Right model the other central role at the LHC is played by the doubly charged scalars [94, 95, 96, 97, 47, 98, 48]. If light enough they have interesting signatures at colliders through their decays into same-sign leptons in the final state. In particular they can be produced with Z/γ^* as intermediate states, see FIG. 3.6. Pair production has the distinctive signature that consists in same-sign dilepton pairs in the final state. Doubly charged scalars belonging to the $SU(2)_L$ triplet, should be discovered at the LHC in the lepton-lepton channel. For 300fb^{-1} of integrated luminosity the mass reach is around 1 TeV. In the W-W channel is around 700 GeV [98]. In [99] a the lower bound for δ_R^{++} of a few hundred GeV (for $v_R \approx 10$TeV) emerges from the scalar masses assuming $v \ll v_R$.

The expression for the decay rate of δ_R^{++} into a lepton pair is

$$\Gamma(\delta_R^{++} \to l_i^+ l_k^+) = \frac{1}{16\pi(1+\delta_{ik})}|(Y'_{\Delta_R})_{ik}|^2 m_{\delta_R^{++}}. \tag{3.25}$$

(no summation convention over repeated indices)

It can also decay into $W_R^+ W_R^+$-pair but this decay is kinetically suppressed if $m_{\delta_R^{++}} \ll m_{W_R}$. In this case δ_R^{++} decays mostly into leptons and the branching ratios are

$$\frac{\Gamma(\delta_R^{++} \to l_i^+ l_k^+)}{\Gamma(\delta_R^{++} \to all)} \equiv \mathrm{Br}(\delta_R^{++} \to l_i^+ l_k^+) = \frac{2}{(1+\delta_{ik})} \frac{|(V_R^* m_N V_R^\dagger)_{ik}|^2}{\sum_{k'} m_{N_{k'}}^2}. \tag{3.26}$$

Notice that they are independent of the δ_R^{++} mass and depend in general on the Majorana phases in K_N.

Using the parametrization of Eq. (2.22) and Eq. (3.26), we compute the branching ratios $\mathrm{Br}(\delta_R^{++} \to e^+e^+)$, $\mathrm{Br}(\delta_R^{++} \to \mu^+e^+)$ and $\mathrm{Br}(\delta_R^{++} \to \mu^+\mu^+)$. In appendix E, we give the explicit formulas for these branching ratios. In FIG. 3.7 we show how the branching ratios depend on the Majorana phases assuming type II dominance and $\mathcal{C}$ as the LR symmetry. We do it for the representative values $\delta = \pi/2$, $m_{N_{lightest}} = 0.5$TeV and $m_{N_{heaviest}} = 1$ TeV, in both normal and inverted neutrino mass hierarchies.

As we can see from FIG. 3.7, the decay rates of δ_R^{++} into electrons and muons are considerably affected by the Majorana phases ϕ_2 and ϕ_3. Notice that when the branching ratio into two electrons and two muons tends to be large, that of one electron and one muon tends to be smaller.

Notice from Eq. (3.26) that there are five independent branching ratios into leptons. Taking into account the KS process, we can see that there are more observables than parameters to be fixed by the experiment (three mixing angles, the Dirac phase δ and the Majorana phases ϕ_2 and ϕ_3). For example, by measuring all the elements of $\hat{V}_R$ through the KS process (as we have explicitly shown) and taking let's say the decays $\delta_R^{++} \to e^+e^+$ and $\delta_R^{++} \to \mu^+\mu^+$, the remaining branching ratios are immediately fixed. This in turn fixes a large number of low-energy experiments, such as the radiative corrections to muon decay and the lepton-flavor-violating decay rates of $\mu \to e\gamma$, $\mu \to eee$ and $\mu \to e$ conversion in nuclei. This is a clear example of the complementary role played by high and low energy experiment in the determination of the left-right symmetric theory [89, 90, 100]. So far we have considered only the decays of δ_R^{++} and not δ_L^{++}. The question is whether one can distinguish them without measuring the polarization of the final leptons. We notice that it can be done at the LHC for $v_L < 10^{-4}$ GeV, i.e in the leptonic decay region for the doubly charged scalar δ_L^{++} (see for instance [47, 48] for detailed studies on this issue). This is due to the relations

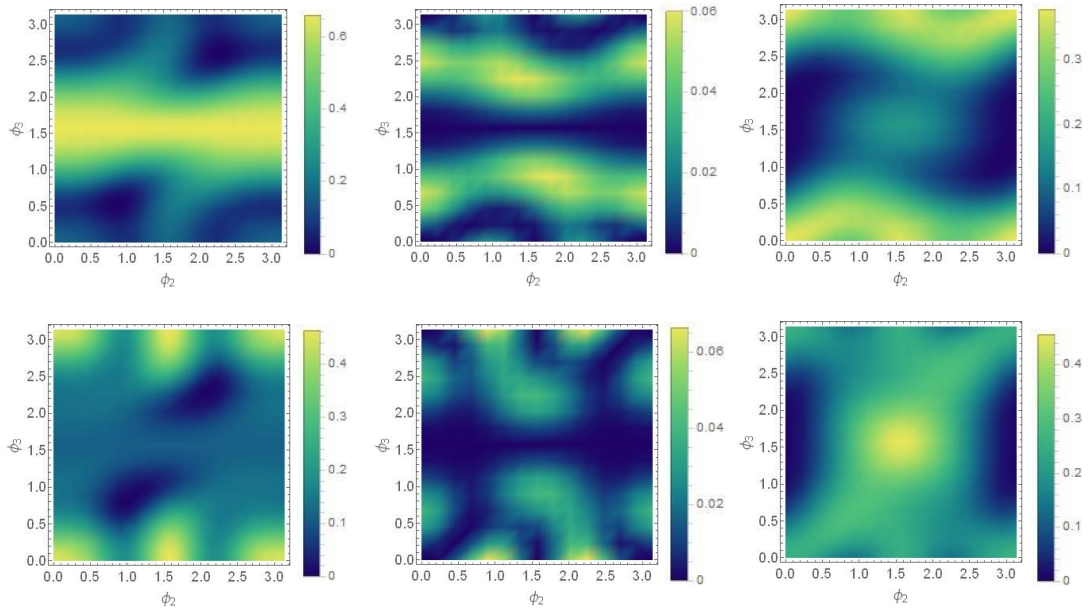

Figure 3.7: Plots for the branching ratios of δ_R^{++} into leptons in the (ϕ_2, ϕ_3) plane. We assume $\delta = \pi/2$ and the masses for the heaviest and lightest right-handed neutrinos, $m_{heaviest} = 1$TeV and $m_{lightest} = 0.5$TeV in type II dominance. (Left) Br($\delta_R^{++} \to e^+e^+$). (Center) Br($\delta_R^{++} \to e^+\mu^+$). (Right) Br($\delta_R^{++} \to \mu^+\mu^+$). (top) Normal hierarchy for neutrino masses. (Bottom) Inverted hierarchy for neutrino masses.

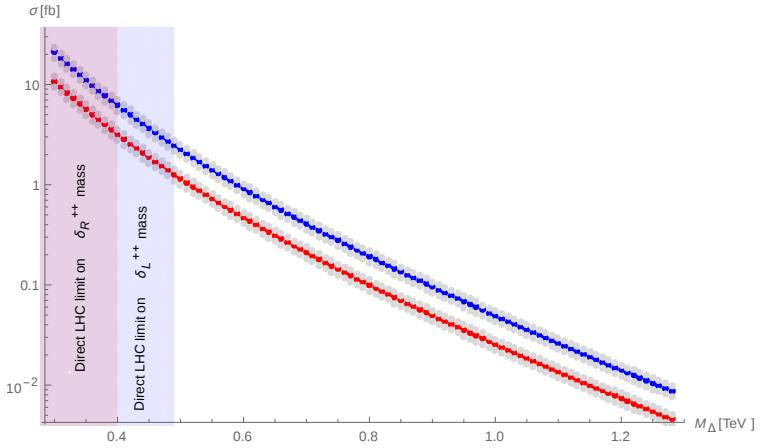

Figure 3.8: Production cross sections for a pair of doubly charged scalars at LHC with 13 TeV center of mass energy as a function of their masses M_Δ. Red line corresponds to δ_R^{++} and blue lines to δ_L^{++} production cross sections. Gray bands show the theoretical uncertainties.

(2.25) and (2.26) and the fact that the production cross section is a factor 2.5 bigger for δ_L^{++} – see Fig. 3.8, than the one for δ_R^{++} [101, 102, 45], where we used the MSTW 2009 [103] PDF sets to compute the cross sections. Of course it is crucial that the backgrounds are negligible after selection criteria are applied [104, 45]. In [101], the next-to-leading order QCD corrections of the production cross-sections at the LHC are calculated and the total theoretical uncertainties are estimated to be $10 - 15\%$.

At this point the reader may well ask about the physical consequences of the phases appearing in K_e. In this respect we notice that lepton dipole moments and CP-odd asymmetries in LFV decays are in general sensitive to them. Therefore we can relate, in principle, all the parameters appearing in V_R with the experiment.

Chapter 4

Time-reversal symmetry violation in several Lepton-Flavor-Violating processes

Lepton Number Violating (LNV) and Lepton Flavor violating (LFV) processes are forbidden in the Standard Model (SM) and are thus a good probe of new physics. In principle new physics brings also new sources of CP violation and therefore time reversal (T) symmetry violation in any local, Lorentz invariant quantum field theory.

Motivated by this we explicitly compute T-odd triple vector correlations for the LFV $\mu \to e\gamma$ decay and $\mu \to e$ conversion process, since much of the present and future experimental efforts are devoted to these two processes.

In the next sections we present the results of the computation of a triple vector correlation in the $\mu \to e\gamma$ decay and $\mu \to e$ conversion process. We perform the computation using the most general effective Hamiltonians describing both processes. As we shall see and in the context of the minimal left-right model these triplet vector correlations may be used to distinguish between parity or charged conjugation as the discrete left-right symmetry.

4.1 Computation of a triple vector correlation in the $\mu \to e\gamma$ decay

T-odd asymmetries in the $\mu \to e\gamma$ were considered in the past. In [25, 26], it was shown that by studying the polarization of electron and the photon coming from the muon decay it is possible to extract the CP-violating phases from the experiment. The conclusion was that in order to extract the CP-violating phases both electron and photon polarizations must be measured. In this thesis instead, we present an alternative way of extracting the CP-violating phases of the effective

Hamiltonian in the $\mu \to e\gamma$ decay. This is complementary to the work presented in [25, 26]. The novelty is that no measurements of the final photon polarizations are needed. We consider the T-violating triple vector product

$$\hat{s}_{\mu^+} \cdot (\hat{p}_{e^+} \times \hat{s}_{e^+}) = \cos\Phi \sin\theta_s, \tag{4.1}$$

where θ_s is the angle between the polarization's direction ($\hat{s}_{e^+}$) of the positron and its momentum's direction $\hat{p}_{e^+}$, Φ is the angle formed between $\hat{s}_{\mu^+}$ and the direction defined by $\vec{p}_{e^+} \times \vec{s}_{e^+}$ and Ψ is the azimuthal angle. In Fig.2.1 the reference frame and setup are shown. Notice that this quantity changes sign under parity and naive time-reversal transformation $\hat{T}$ defined by $t \to -t$. For processes whose interactions are characterized by a small coupling, it can be shown at first order that the connected part of the S-matrix is hermitian [27] and therefore the violation of the $\hat{T}$ symmetry amounts the violation of the time-reversal symmetry.

We define the triple vector correlation as

$$\langle \hat{s}_{\mu^+} \cdot (\hat{p}_{e^+} \times \hat{s}_{e^+}) \rangle_\Phi \equiv \frac{N(\cos\Phi > 0) - N(\cos\Phi < 0)}{N_{total}} = \frac{\int_0^\pi d\Phi d\Gamma/d\Phi \cdot \mathrm{sgn}(\hat{s}_{\mu^+} \cdot (\hat{p}_e \times \hat{s}_{e^+}))}{\Gamma_{total}}, \tag{4.2}$$

where Γ_{total} and N_{total} are the total decay rate and the total number of events for the initially polarized muon respectively, $N(\cos\Phi > 0)$ and $N(\cos\Phi < 0)$ are the number of events satisfying $\cos\Phi > 0$ and $\cos\Phi < 0$ respectively.

The 4-momenta of the participating particles in the rest frame of the muon are given by

$$p^\mu_{\mu^+} = (m_\mu, 0, 0, 0), \tag{4.3}$$

$$p^\mu_{e^+} = (E_e, |\vec{p}_{e^+}| \sin\theta_s, |\vec{p}_{e^+}| \cos\theta_s, 0), \tag{4.4}$$

$$p^\mu_\gamma = (E_\gamma, -|\vec{p}_{e^+}| \sin\theta_s, -|\vec{p}_{e^+}| \cos\theta_s, 0) \tag{4.5}$$

where the mass of the positron has been neglected. The energy E_{e^+} of the positron and the energy E_γ of the photon are given by

$$E_{e^+} \cong E_\gamma = |\vec{p}_{e^+}| = \frac{m_\mu}{2}. \tag{4.6}$$

From the effective Hamiltonian in eqn. (2.35) and eqns. (F.1), (F.4) and (F.5) in appendix F, a straightforward computation gives the following value for the correlation

$$\langle \hat{s}_{\mu^+} \cdot (\hat{p}_{e^+} \times \hat{s}_{e^+}) \rangle_\Phi = \sin\theta_s \frac{\Im m(A_L A_R^*)}{|A_L|^2 + |A_R|^2}. \tag{4.7}$$

The main advantage of this quantity is that no measurements of the photon polarizations are needed.

In summary we find that given a source of polarized anti-muons, by measuring the 3-momentum $\vec{p}_{e^+}$ of the outgoing positron and its polarization $\vec{s}_{e^+}$, the asymmetry shown in eqn. (4.7) is sensitive to the CP-violating phases of the effective Hamiltonian shown in (2.35). In [105, 106, 107, 108, 109] it is shown that measurements of the polarization of electrons coming from the muon decay are feasible. We assume a 100 % polarized muon flux so that our results must be trivially rescaled by the actual polarization of the initial muons.

4.2 Computation of a triple vector correlation in the $\mu \to e$ conversion process

Following the same lines of the last section, we define an asymmetry given by comparing the number of events with $\vec{s}_\mu \cdot (\vec{p}_e \times \vec{s}_e) > 0$ with the ones satisfying $\vec{s}_\mu \cdot (\vec{p}_e \times \vec{s}_e) < 0$ in the $\mu \to e$ conversion process and it is of the form

$$\begin{aligned} \langle \hat{s}_\mu \cdot (\hat{p}_e \times \hat{s}_e) \rangle_\Phi &\equiv \frac{N(\cos\Phi > 0) - N(\cos\Phi < 0)}{N_{total}} \\ &= \frac{\omega_{conv}(\cos\Phi > 0) - \omega_{conv}(\cos\Phi < 0)}{\omega_{conv}}, \end{aligned} \tag{4.8}$$

where ω_{conv} is the total conversion rate and as previously, Φ is the angle between the plane formed by the vectors $\hat{p}_e$ and $\hat{s}_e$ and the polarization of the muon $\hat{s}_\mu$. We used the same coordinate system shown in Fig.2.1 but clearly there is no photon coming from the muon decay.

A direct computation gives [1]

$$\omega_{\rm conv}(\cos\Phi>0)-\omega_{\rm conv}(\cos\Phi<0)=R^2\int d\Omega\cdot{\rm sgn}(\hat{s}_\mu\cdot(\hat{p}_e\times\hat{s}_e))\cdot\psi^\dagger_{as}P_e^{(+)}\psi_{as}$$
$$=\frac{1}{2}G_F^2\sin\theta_s\Re e[e^{i(\delta_{-1}-\delta_{+1})}(C_R-C_L)((C_R^*+C_L^*))]=G_F^2\sin\theta_s\Im m(C_LC_R^*)+\mathcal{O}(\alpha Z)$$
$$+\mathcal{O}(\frac{m_e}{E_e}), \tag{4.9}$$

where

$$C_R\equiv DA_R+S^{(p)}(\tilde{g}^{(p)}_{LS}+\tilde{g}^{(p)}_{LV})+S^{(n)}(\tilde{g}^{(n)}_{LS}+\tilde{g}^{(n)}_{LV}), \tag{4.10}$$

$$C_L\equiv DA_L+S^{(p)}(\tilde{g}^{(p)}_{RS}+\tilde{g}^{(p)}_{RV})+S^{(n)}(\tilde{g}^{(n)}_{RS}+\tilde{g}^{(n)}_{RV}) \tag{4.11}$$

and

$$\tilde{g}^{(p)}_{LS,RS}\equiv\sum_q G^{(q,p)}g_{LS,RS(q)},\qquad \tilde{g}^{(n)}_{LS,RS}\equiv\sum_q G^{(q,n)}g_{LS,RS(q)}, \tag{4.12}$$

$$\tilde{g}^{(p)}_{LV,RV}\equiv 2g_{LV,RV(u)}+g_{LV,RV(d)},\qquad \tilde{g}^{(n)}_{LV,RV}\equiv g_{LV,RV(u)}+2g_{LV,RV(d)}. \tag{4.13}$$

D, $S^{(n,p)}$ are nuclear constants already calculated and tabulated in [72] for various elements. $G^{(q,p)}$ and $G^{(q,n)}$ are obtained from the scalar matrix element [75, 72]

$$\langle N|\bar{q}q|N\rangle=ZG^{(q,p)}\rho^{(p)}+(A-Z)G^{(q,n)}\rho^{(n)} \tag{4.14}$$

Z and A are the atomic and mass number respectively, $\rho^{(n)}$ and $\rho^{(p)}$ are the neutron and proton densities inside the nucleus. Notice that in the high energy limit the Coulomb phases satisfy

$$\delta_{-1}-\delta_{+1}=\frac{\pi}{2}+\mathcal{O}(\frac{\alpha Z}{E_e}). \tag{4.15}$$

The Coulomb phases $\delta_{\pm1}$ are defined in Eq. (2.49) and $d\Omega$ is given by $d\Omega=d\Psi d\Phi\sin\Phi$.

Finally the asymetry shown in Eq. (4.8) takes the form

$$\langle\hat{s}_\mu\cdot(\hat{p}_e\times\hat{s}_e)\rangle_\Phi=\frac{1}{2}\sin\theta_s\frac{\Im m(C_LC_R^*)}{|C_L|^2+|C_R|^2}+\mathcal{O}(\alpha Z)+\mathcal{O}(\frac{m_e}{E_e}). \tag{4.16}$$

where m_e is the electron mass.

[1] For more details see section 2.4.3 and 2.4.4.

The expression obtained is valid for non-relativistic muons and we droped terms of the order αZ and m_e/E_e. In practice equation (4.16) must be multiplied by the polarization of the initial muons, which is of the order of 15% in the conversion process [110].

In deriving the expression for the asymmetry in the conversion process we make use of the expression for the total conversion rate, which is

$$\omega_{conv} = R^2 \int d\Omega \psi^{\dagger}_{as}\psi_{as} = 2\pi \left(\frac{1}{2} \sum_{\kappa,\mu} |\langle \psi^{\mu}_{\kappa} | H_{eff} | \psi_i \rangle|^2 \right) = 2G_F^2(|C_L|^2 + |C_R|^2) \tag{4.17}$$

and it is complete agreement with the expression for the total conversion rate reported in [72].

4.3 Triplet vector correlations in the minimal Left-Right theory

As a concrete example of a theory beyond the SM that gives order one values for the T-odd triple vector correlation [28] we consider the minimal LR symmetric model. In what follows we analyze separately the contributions to the asymmetries (4.7) and (4.16) in the case of $\mathcal{P}$ and $\mathcal{C}$ as the LR symmetries. In [28] it is found that this contribution can be of order one, since there are new contributions coming from interactions of charged leptons with the singly-charged and doubly-charged scalar fields.

4.3.1 $\mu \to e\gamma$ decay

In this section and for the $\mu \to e\gamma$ decay, we study the contributions to the triple vector correlation for both Parity and Charge Conjugation as the LR symmetry.

Parity as the LR symmetry: in [111] the authors presented a complete study of the contributions to several LFV processes in the context of the minimal LR extension of the SM and it is found that the branching ratio for this process is of the form

$$\mathrm{Br}(\mu \to e\gamma) = 384\pi^2 e^2(|A_L|^2 + |A_R|^2) \tag{4.18}$$

where

$$A_R = \frac{1}{16\pi^2}\sum_n (V_R^\dagger)_{en}(V_R)_{n\mu}[\frac{m_W^2}{m_{W_R}^2}S_3(X_n) - \frac{X_n}{3}\frac{m_W^2}{m_{\delta_R^{++}}^2}], \tag{4.19}$$

$$A_L = \frac{1}{16\pi^2}\sum_n (V_R^\dagger)_{en}(V_R)_{n\mu}X_n[-\frac{1}{3}\frac{m_W^2}{m_{\delta_L^{++}}^2} - \frac{1}{24}\frac{m_W^2}{m_{H_1^+}^2}] + \mathcal{O}(\tan 2\beta \sin\alpha), \tag{4.20}$$

$$X_n = (\frac{m_N}{m_{W_R}})^2, \quad S_3(x) = -\frac{x}{8}\frac{1+2x}{(1-x)^2} + \frac{3x^2}{4(1-x)^2}[\frac{x}{(1-x)^2}(1-x+\log x)+1]. \tag{4.21}$$

m_{N_n} are the heavy neutrino masses where $n = 1, 2, 3$. m_W is the W boson mass, m_{W_R} is the W_R boson mass, $m_{H_1^+}$ is the mass of the heavy scalar H_1^+ and $m_{\delta^{++}_{(L,R)}}$ are the masses for the left and right doubly charged scalars respectively and we use m_ν to denote the light neutrino masses.

Notice that the loop function S_3 is always small as far as m_N is not much bigger than m_{W_R}, so that the term with the loop function can neglected for a wide range of the heavy neutrino masses (see figure 4.1) and therefore the correlation defined in (4.7) is suppressed. Finally we neglect the contribution of the charged Higgs H_1^+ since its mass cannot be lower than (15-20) TeV [40, 41]. This poses no problem for the theory, since its mass emerges at the large scale of symmetry breaking [5, 112]. The gauge boson and doubly-charged scalar masses can be obtained at the LHC through the so called KS process and the decays of the doubly charged scalars in addition with all the mixing angles and the Dirac phase in V_R. This is an example of the complementary role played by the high and low energy experiments in the establishment of the LR theory [89, 100, 113, 114, 115, 116, 117].

For the sake of illustration, imagine that type II see-saw is the dominant source of neutrino masses i.e. $\frac{M_N}{\langle\Delta_R\rangle} = \frac{M_\nu}{\langle\Delta_L\rangle}$ and $V_L = V_R$. In this case it is possible to show that the heavy neutrino masses satisfy the relation [89]

$$\frac{m_{N_2}^2 - m_{N_1}^2}{m_{N_3}^2 - m_{N_1}^2} = \frac{m_{\nu_2}^2 - m_{\nu_1}^2}{m_{\nu_3}^2 - m_{\nu_1}^2} \simeq \pm 0.03, \tag{4.22}$$

where the $\pm$ corresponds to normal (NH) and inverted (IH) neutrino mass hierarchy respectively. In what follows we denote m_{N_0} the lightest right-handed neutrino mass, m_{N_H} the heaviest right-handed neutrino mass and δ is the Dirac phase present in $\hat{V}_R$. In Fig. 4.2 and for the two representative values of $m_{N_H} = 0.5$ TeV and $m_{N_H} = 1$ TeV we show the allowed region obtained from the MEG

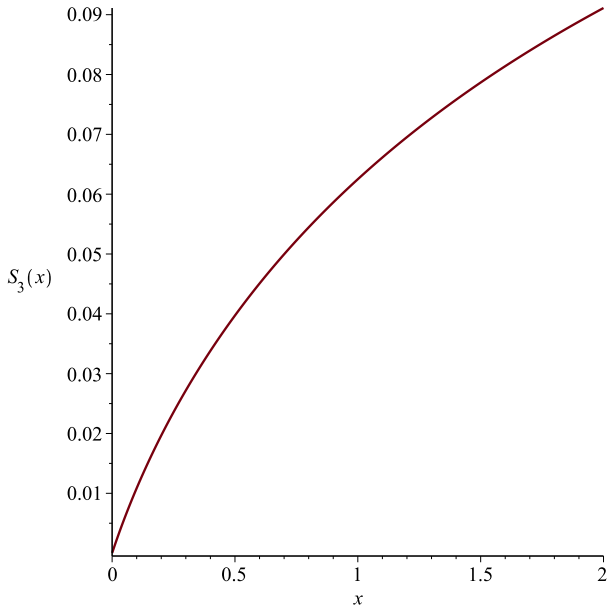

Figure 4.1: Plot of the loop function $S_3(x)$.

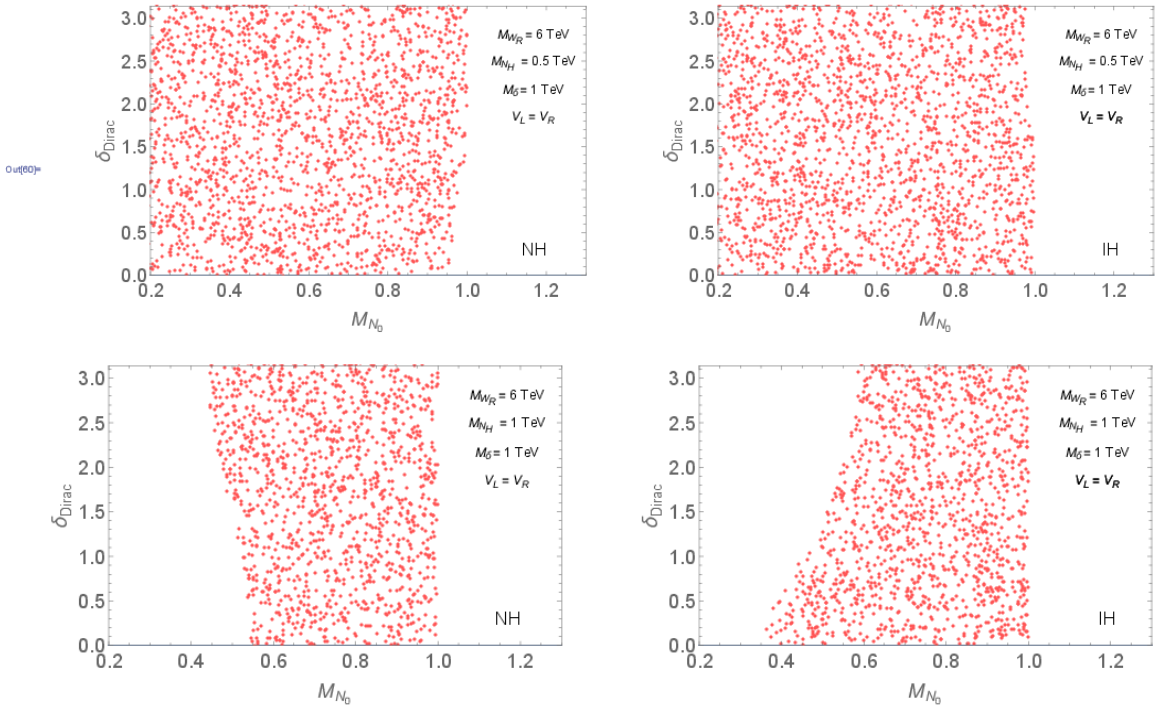

Figure 4.2: Plot obtained by considering the MEG bound shown in Eq. (1.1). (Right) Normal hierarchy case (NH). (Left) Inverse hierarchy case (IH). The colored region is the allowed one. (Top) Mass of the heaviest right-handed neutrino $m_{N_H} = 0.5$ TeV. (Bottom) Mass of the heaviest right-handed neutrino $m_{N_H} = 1$ TeV.

bound in the $\{m_{N_0}, \delta_{\rm Dirac}\}$ plane, for both normal and inverted neutrino mass spectrum. The region for $m_{N_H} = \{0.5 - 1\}$ gives rise to the exciting LNV signals at the LHC trough the KS process. Consistent with the perturbativity bounds obtained in [34], we assume $m_{W_R} = 6$ TeV and common masses for the doubly charged scalars $m_{\delta_L^{++}} = m_{\delta_R^{++}} = m_\delta = 1$ TeV. The reader may ask about the very different behavior obtained for the two values of the heaviest neutrino mass chosen, and the point is that this can be readily understood by noticing that the amplitude is approximately proportional to $|\Delta m^2_{13}| = |m^2_{N_H} - m^2_{N_0}|$, so that a bound is obtained for $|\Delta m^2_{13}|$ rather on the lightest neutrino mass itself.

In figure 4.3 (top) we plot the absolute value for the triple vector correlation given in (4.7) in the (m_{N_0}, δ)-plane, where one may see that the values of the correlation (4.7) goes from 10^{-6} to 10^{-5} in the allowed region.

One would be tempted to conclude that the triple vector correlation may be bigger for general values of neutrino masses and mixings. However from eqns. (2.26), the contribution to the triple vector correlation shown in (4.7) is bounded to be less 10^{-2} since $\tan 2\beta \sin\alpha < 10^{-2}$ from the quark masses [40, 38, 17]. The point is that for charged leptons masses (M_l) bigger or equal than the Dirac mass of neutrinos (M_D), the mass matrix of the charged leptons is nearly hermitian leading therefore to nearly equal leptonic left and right mixing matrices. This is in complete analogy to the situation in the quark sector studied in [32, 40]. Of course it is possible to assume that the elements of the Dirac mass matrix $M_D > M_l$, but we will not pursue this possibility since in this case the original see-saw mechanism would lose its meaning and one would have to invoke accidental cancellations in order to explain the smallness neutrino masses.

Charge conjugation as the LR symmetry: from eqn. (2.25) we have that

$$A_R = \frac{1}{16\pi^2}\sum_n (V_R^\dagger)_{en}(V_R)_{n\mu}[\frac{m_W^2}{m_{W_R}^2}S_3(X_n) - \frac{X_n}{3}\frac{m_W^2}{m^2_{\delta_R^{++}}}], \tag{4.23}$$

$$A_L = \frac{1}{16\pi^2}\sum_n (V_R^T)_{en}(V_R^*)_{n\mu}X_n[-\frac{1}{3}\frac{m_W^2}{m^2_{\delta_L^{++}}} - \frac{1}{24}\frac{m_W^2}{m^2_{H_1^+}}]. \tag{4.24}$$

Notice that some of the external phases appearing in V_R do not cancel in (4.7) and the triple vector correlation is proportional to $e^{2(\phi_\mu - \phi_e)}$, so that the triple vector correlation is not suppressed

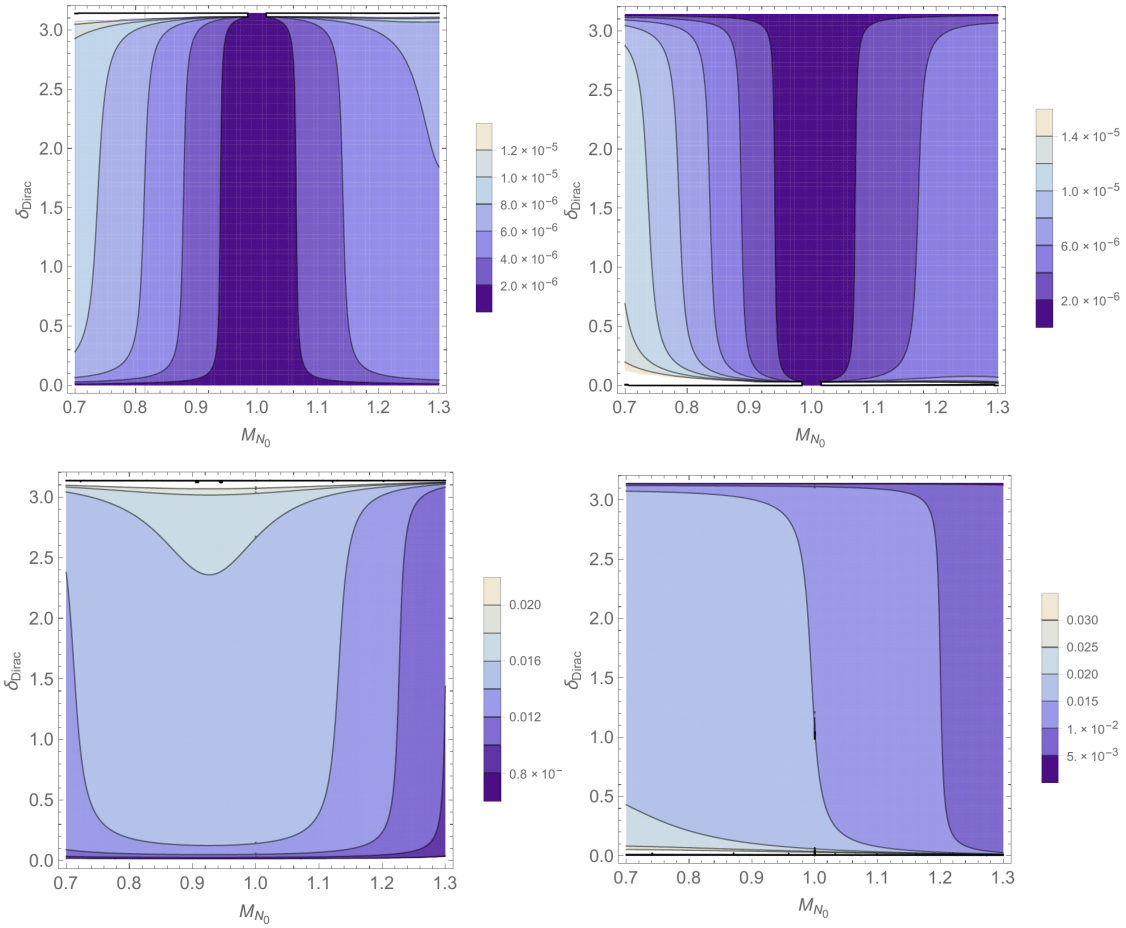

Figure 4.3: (Top) Contour plots illustrating the absolute value of the asymmetry defined in (4.7) as a function of the lightest neutrino mass m_{N_0} and the Dirac phase δ for $\mathcal{P}$ as the LR symmetry. (Bottom) Contour plots illustrating the value of the asymmetry defined in (4.7) as a function of the lightest neutrino mass m_{N_0} and the Dirac phase δ (assuming $\phi_\mu - \phi_e = 0$) for $\mathcal{C}$ as the LR symmetry. (Left) Normal hierarchy for neutrino masses. (Right) Inverse hierarchy for neutrino masses. We take the gauge boson mass $m_{W_R} = 6$TeV, the heaviest right-handed neutrino mass $m_{N_H} = 1$TeV and common masses for the doubly charged scalars of $m_\delta = 1$ TeV. The mixing angles are $\theta_{12} \simeq 33.6^o$, $\theta_{23} \simeq 41.9^o$, $\theta_{13} \simeq 8.7^o$.

by the small θ_{13} mixing-angle. In Fig.4.3 (bottom) we show the absolute value of the triple vector correlation in the (m_{N_0}, δ)-plane. We take $(\phi_\mu - \phi_e) = 0$ in both normal and inverted neutrino mass hierarchies. For $(\phi_\mu - \phi_e) = \pi/4$ it will reach in maximum value of around 0.5 in almost all the parameter space

Finally from Fig.4.3 (bottom) we conclude that $\mathcal{C}$ as the LR symmetry gives larger contributions to the triple vector correlation and this because in the parity case, the triple vector correlation is suppressed due to the near equality between the Yukawa couplings.

The bottom line is that in the most interesting region of the parameter space, a value for the triple vector correlation bigger than 10^{-2} can only be the consequence of $\mathcal{C}$ as the LR symmetry.

One may ask whether this value for the asymmetry of could be measured in forthcoming experiments. Suppose that $\mu \to e\gamma$ is found to be of the order of 10^{-14}. In the best scenario due to the future experimental improvements on the sensitivity, it would become possible to observed at most 10^4 events and out of these events one has to select the ones that have $\theta_s \neq 0$ or $\theta_s \neq \pi$. Moreover suppose that only the events satisfying $\pi/6 < \theta_s < \pi/3$ may be identify in the experiment due to its intrinsic sensitivity. This would imply that we end up having $10^4 \int_{\pi/6}^{\pi/3} \sin\theta_s d\theta_s \sim 10^3$ events in the most optimistic situation. Hence this naive argument allow us to conclude that in most optimistic scenario, an asymmetry of the order 10^{-3} or bigger would probably be seen in the next round of $\mu \to e\gamma$ decay experiments.

4.3.2 $\mu \to e$ conversion process

In this section we consider the triple vector correlation for the $\mu \to e$ conversion process in the context of the minimal LR symmetric extension of the SM where the relevant branching ratio is given by [111]

$$\omega_{conv}(\mu \to e) = \frac{2G_F^2 V^{(p)2}}{\Gamma_{\text{capt}}} \left(\frac{\alpha^2}{16\pi^2}\right) \left(|F_L^{(\gamma)}|^2 + |F_R^{(\gamma)}|^2\right). \tag{4.25}$$

The values of the capture rate Γ_{capt} are tabulated in [118] for several elements. In [111] it was shown that the contribution of the doubly-charged scalar may dominate due to a logarithmic enhancement

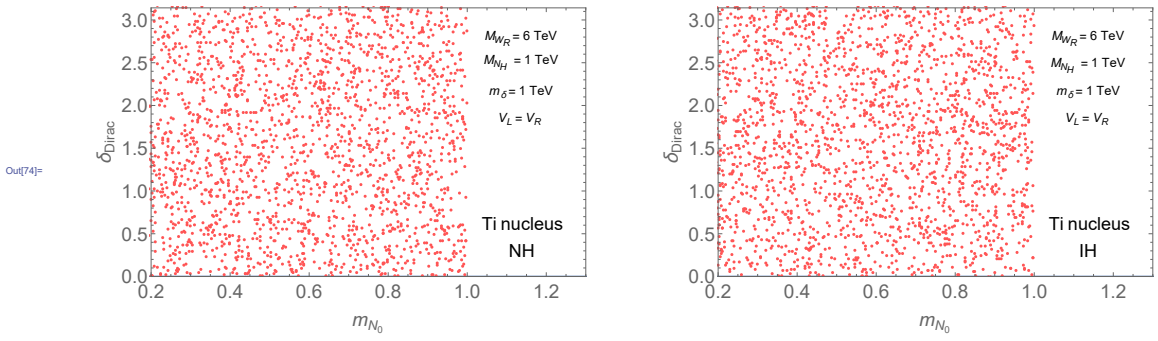

Figure 4.4: Plot obtained by considering the SINDRUM II bound for Titanium shown in Eq. (1.2). (Right) Normal hierarchy case (NH). (Left) Inverse hierarchy case (IH). The colored region is the allowed one. We take the mass of the heaviest right-handed neutrino $m_{N_H} = 1$ TeV.

and in this case the functions $F_L^{(\gamma)}$ and $F_R^{(\gamma)}$ may be written as

$$F_{(L,R)}^{(\gamma)} \simeq 128\pi^2 A_{(L,R)} \log(m_\mu^2/m_{\delta^{++}_{(L,R)}}^2). \tag{4.26}$$

For completeness we show in Fig. 4.4 the allowed region obtained by considering the SINDRUM bound for Titanium shown in Eq. (1.2) assuming the same values for the heavy neutrino masses of the last section. As we can see from the figure for $m_{W_R} = 6$ TeV the SINDRUM II collaboration gives no bound in the region considered for both NH and IH cases. From Eq. (4.26) and assuming that the dominant terms are the logarithmic enhance ones, the amplitude for the conversion process and the $\mu \to e\gamma$ decay are proportional. Therefore a similar qualitative behavior is obtained. We can see that the bound obtained is similar to the one of the $\mu \to e\gamma$ experiment and this is due to the fact that the logarithmic enhancement in Eq. (4.26) compensate the α suppression in the conversion rate [111]. For Gold the bound one would obtain is similar since the ratio between the conversion rates for the two elements is around 0.83. On the other hand, for the gold atom relativistic effects of the muon becomes relevant, so that the result shown in Eq. (4.16) cannot be trusted in this case.

Finally the asymmetry defined in Eq. (4.16) takes the form

$$\langle \vec{s}_\mu \cdot (\vec{p}_e \times \vec{s}_e) \rangle_\Phi = \frac{\sin\theta_s}{2} \frac{\Im m(F_L^{(\gamma)} F_R^{*(\gamma)})}{|F_L^{(\gamma)}|^2 + |F_R^{(\gamma)}|^2} = \frac{\sin\theta_s}{2} \frac{\Im m(A_L A_R^*)}{|A_L|^2 + |A_R|^2}, \tag{4.27}$$

where it can be seen that this asymmetry has the same flavor structure of the coefficients A_L and

A_R defined previously for the $\mu \to e\gamma$ decay, therefore the same conclusion obtained in the $\mu \to e\gamma$ case holds for the $\mu \to e$ conversion process as well.

Regarding the expected sensitivity for the conversion process the arguments we used in the $\mu \to e\gamma$ decay apply, but with the difference that the final sensitivity is rescaled by a factor of the order of 10^{-1} due to the depolarization –around 15%– of the muons in the conversion process [110].

Chapter 5

Conclusions

In the context of the minimal Left-Right symmetric theory, we studied the determination of the leptonic right-handed mixing matrix V_R at the LHC. We considered the Keung-Senjanović process and the decay of the doubly charged scalar δ_R^{++}.

For non-degenerate heavy neutrino masses, the KS process is sensitive to 3 mixing angles and the Dirac-type phase. We proposed a simple approach in order to determine the three mixing angles and the Dirac phase present in V_R and find explicit and simple conditions for their determination. We noticed that for a complete determination of the right-handed leptonic mixing matrix, at least 2 heavy neutrinos must be produced on-shell. In this case the inclusion of tau-leptons in the analysis is mandatory. For three heavy neutrinos on-shell the three mixing angles and the Dirac phase may be determined by measuring electrons and muons in the final state, rendering the three heavy neutrino case ideal for the LHC. We found exact analytical solutions for the mixing angles and the Dirac phase δ in terms of measurable quantities at the LHC in both two and three heavy neutrino cases. We also show that the hadronization effects for the final jets are under control, thus rendering the proposed strategy feasible at the LHC. Finally we find that for two heavy neutrino at the LHC with masses near or below the TeV, an integrated luminosity of 63 fb^{-1} is required in order to measure the three mixing angles that parametrize the right handed leptonic mixing matrix. The required luminosity rises to 446 fb^{-1} once detector simulation is included (assuming 50 % of tau identification). In the case of three heavy neutrinos at the LHC and for the range of heavy neutrino masses considered (near or below the TeV) a luminosity of 417 fb^{-1} and 385 fb^{-1} is required for

both normal and inverted neutrino mass hierarchy respectively. Finally, these luminosities rise from 417 fb^{-1} to 1190 fb^{-1}, and from 385 fb^{-1} 1100 fb^{-1} once detector simulation is included. Our main focus was the LHC but the strategy is applicable in any hadron collider and we hope that it could be useful in the foreseen future and the next generation of hadron colliders.

For degenerate heavy neutrinos masses, the lepton-number-violating, same-sign lepton channel (FIG. 2.1. Bottom) is in general sensitive to two of the Majorana phases of V_R, because in this case there are interference terms between the degenerate right-handed neutrino mass eigenstates.

We point out that the decays of the doubly charged scalar δ_R^{++} into leptons are significantly affected by the same two Majorana phases. In FIG. 4.1 we show its branching ratios into e^+e^+,$e^+\mu^+$ and $\mu^+\mu^+$. We did it for $\mathcal{C}$ as the Left-Right symmetry assuming type II see-saw dominance. We considered some representative values of the Dirac phase δ and the right-handed neutrino masses, in both normal and inverted neutrino mass hierarchies.

As a consequence of the near equality of the Yukawa couplings of the doubly charged scalars in both parity or charged conjugation as the Left-Right symmetry, the LHC experiment may distinguish δ_L^{++} from δ_R^{++} without measuring the polarization of the final-state leptons coming from their decays.

Then we focus in the time-reversal symmetry violation in the $\mu \to e\gamma$ decay and the $\mu \to e$ conversion and managed to derive analytical expressions for a T-odd triple vector correlation. We found simple results in terms of the CP-violating phases of the effective Hamiltonians and the expression obtained in the $\mu \to e$ conversion omits relativistic corrections for the muons, but is otherwise complete. For the $\mu \to e\gamma$ decay we conclude that in order to extract the CP violating phases of the theory from the experiment, no measurements of the photon polarizations are needed.

Then as an example of a theory that leads order one values for the triple vector correlation we consider the TeV scale, minimal Left-Right symmetric extension of the SM. Remarkably, due to the relation between left and right Yukawa couplings in (2.23) –see also eqs. (2.25) and (2.26)– this triple vector correlation can be used to discriminate between charge-conjugation or parity as the Left-Right symmetry. More precisely, if the Dirac masses of heavy neutrinos smaller or of the order of the masses of the charge leptons, a value for the triple vector correlation bigger than 10^{-2} can

only be the consequence of charge-conjugation as the Left-Right symmetry.

Appendix A

Scalar potential of the minimal LR model

In this appendix we give the expressions for the scalar potentials for $\mathcal{P}$ and $\mathcal{C}$ as the LR symmetry and are given by [8, 31, 32, 15, 33, 34, 35, 36]

$$
\begin{aligned}
&V_P = -\mu_1^2 \mathrm{Tr}(\Phi^\dagger\Phi) - \mu_2^2[\mathrm{Tr}(\tilde{\Phi}\Phi^\dagger) + \mathrm{Tr}(\tilde{\Phi^\dagger}\Phi)] - \mu_3^2[\mathrm{Tr}(\Delta_L\Delta_L^\dagger) + \mathrm{Tr}(\Delta_R\Delta_R^\dagger)] + \lambda_1[\mathrm{Tr}(\Phi^\dagger\Phi)]^2 \\
&\lambda_2[\mathrm{Tr}^2(\tilde{\Phi}\Phi^\dagger) + \mathrm{Tr}^2(\tilde{\Phi^\dagger}\Phi)] + \lambda_3[\mathrm{Tr}(\tilde{\Phi}\Phi^\dagger)\mathrm{Tr}(\tilde{\Phi^\dagger}\Phi)] + \lambda_4\mathrm{Tr}(\Phi^\dagger\Phi)[\mathrm{Tr}(\tilde{\Phi}\Phi^\dagger) + \mathrm{Tr}(\tilde{\Phi^\dagger}\Phi)] \\
&\rho_1\{\mathrm{Tr}^2(\Delta_L\Delta_L^\dagger) + \mathrm{Tr}^2(\Delta_R\Delta_R^\dagger)\} + \rho_2[\mathrm{Tr}(\Delta_L\Delta_L)\mathrm{Tr}(\Delta_L^\dagger\Delta_L^\dagger) + \mathrm{Tr}(\Delta_R\Delta_R)\mathrm{Tr}(\Delta_R^\dagger\Delta_R^\dagger)] \\
&\rho_3[\mathrm{Tr}(\Delta_L\Delta_L^\dagger)\mathrm{Tr}(\Delta_R\Delta_R^\dagger)] + \rho_4[\mathrm{Tr}(\Delta_L\Delta_L)\mathrm{Tr}(\Delta_R^\dagger\Delta_R^\dagger) + \mathrm{Tr}(\Delta_L^\dagger\Delta_L^\dagger)\mathrm{Tr}(\Delta_R\Delta_R)] \\
&\alpha_1\mathrm{Tr}(\Phi^\dagger\Phi)[\mathrm{Tr}(\Delta_L\Delta_L^\dagger) + \mathrm{Tr}(\Delta_R\Delta_R^\dagger)] + \{\alpha_2 e^{ic}[[\mathrm{Tr}(\tilde{\Phi}\Phi^\dagger)\mathrm{Tr}(\Delta_L\Delta_L^\dagger) + \mathrm{Tr}(\tilde{\Phi^\dagger}\Phi)\mathrm{Tr}(\Delta_R\Delta_R^\dagger)] + h.c\} \\
&\alpha_3[\mathrm{Tr}(\Phi\Phi^\dagger\Delta_L\Delta_L^\dagger) + \mathrm{Tr}(\Phi^\dagger\Phi\Delta_R\Delta_R^\dagger)] \\
&+ \beta_1[\mathrm{Tr}(\Phi\Delta_R\Phi^\dagger\Delta_L^\dagger) + \mathrm{Tr}(\Phi^\dagger\Delta_L\Phi\Delta_R^\dagger)] + \beta_2[\mathrm{Tr}(\tilde{\Phi}\Delta_R\Phi^\dagger\Delta_L^\dagger) + \mathrm{Tr}(\tilde{\Phi}^\dagger\Delta_L\Phi\Delta_R^\dagger)] \\
&+ \beta_3[\mathrm{Tr}(\Phi\Delta_R\tilde{\Phi}^\dagger\Delta_L^\dagger) + \mathrm{Tr}(\Phi^\dagger\Delta_L\tilde{\Phi}\Delta_R^\dagger)] \qquad \text{(A.1)}
\end{aligned}
$$

$$V_C = -\mu_1^2 \mathrm{Tr}(\Phi^\dagger \Phi) - \mu_2^2 [\mathrm{Tr}(\tilde{\Phi^\dagger} \Phi) + h.c.] - \mu_3^2 [\mathrm{Tr}(\Delta_L \Delta_L^\dagger) + \mathrm{Tr}(\Delta_R \Delta_R^\dagger)] + \lambda_1 [\mathrm{Tr}(\Phi^\dagger \Phi)]^2$$

$$\lambda_2 [e^{id_2} \mathrm{Tr}^2(\tilde{\Phi} \Phi^\dagger) + h.c.] + \lambda_3 [\mathrm{Tr}(\tilde{\Phi} \Phi^\dagger) \mathrm{Tr}(\tilde{\Phi^\dagger} \Phi)] + \lambda_4 \mathrm{Tr}(\Phi^\dagger \Phi) [e^{id_4} \mathrm{Tr}(\tilde{\Phi} \Phi^\dagger) + h.c.]$$

$$\rho_1 \{\mathrm{Tr}^2(\Delta_L \Delta_L^\dagger) + \mathrm{Tr}^2(\Delta_R \Delta_R^\dagger)\} + \rho_2 [\mathrm{Tr}(\Delta_L \Delta_L) \mathrm{Tr}(\Delta_L^\dagger \Delta_L^\dagger) + \mathrm{Tr}(\Delta_R \Delta_R) \mathrm{Tr}(\Delta_R^\dagger \Delta_R^\dagger)]$$

$$\rho_3 [\mathrm{Tr}(\Delta_L \Delta_L^\dagger) \mathrm{Tr}(\Delta_R \Delta_R^\dagger)] + \rho_4 [e^{ir_4} \mathrm{Tr}(\Delta_L^\dagger \Delta_L^\dagger) \mathrm{Tr}(\Delta_R \Delta_R) + h.c.]$$

$$\alpha_1 \mathrm{Tr}(\Phi^\dagger \Phi) [\mathrm{Tr}(\Delta_L \Delta_L^\dagger) + \mathrm{Tr}(\Delta_R \Delta_R^\dagger)] + \alpha_2 \{(e^{ic} \mathrm{Tr}(\tilde{\Phi} \Phi^\dagger) + h.c.)(\mathrm{Tr}(\Delta_L \Delta_L^\dagger) + \mathrm{Tr}(\Delta_R \Delta_R^\dagger)] + h.c)\}$$

$$\alpha_3 [\mathrm{Tr}(\Phi \Phi^\dagger \Delta_L \Delta_L^\dagger) + \mathrm{Tr}(\Phi^\dagger \Phi \Delta_R \Delta_R^\dagger)] + \beta_1 [e^{ib_1} \mathrm{Tr}(\Phi \Delta_R \Phi^\dagger \Delta_L^\dagger) + h.c.]$$

$$+ \beta_2 [e^{ib_2} \mathrm{Tr}(\tilde{\Phi} \Delta_R \Phi^\dagger \Delta_L^\dagger) + h.c.] + \beta_3 [e^{ib_3} \mathrm{Tr}(\Phi \Delta_R \tilde{\Phi}^\dagger \Delta_L^\dagger) + h.c.] \tag{A.2}$$

Appendix B

Mass reach for Z_R at the LHC with 13 TeV of center of mass energy

An interesting question would be what is the mass reach for Z_R at the LHC?. Following the procedure of [119] a simple lepton isolation procedure was used in order to select the events. This procedure consist on using the sum of the p_T of all particles in a cone $\Delta R = \sqrt{\Delta\eta + \Delta\Phi} = 0.3$ around the lepton, divided by the lepton p_T, i.e,

$$R \equiv \frac{\sum_{\Delta R<0.3} p_T^{particles}}{p_T^{lepton}} \tag{B.1}$$

Using Madgraph 5 [77] for the parton level generation of events and h Pythia 6 [78] for hadronization of the final states, we perform the simulation for both the signal and the backgrounds for this process. Therefore for each lepton we are going to use $p_T > 20$ GeV and $\Delta R < 0.05$ in order to be sure that the two leptons come from the Z_R decay –see Fig. B.1 for a comparison of $\Delta R < 0.05$ for the signal with the main backgrounds. Since we are interested in the high mass region for Z_R we also consider the invariant mass of the two leptons coming from the Z_R decay bigger than 1TeV ($m_{ll} > 1$TeV). The backgrounds are found to be negligible in the high mass region for the two leptons (i.e the 5 σ deviation from the background is reach much faster than let say 10 events), therefore we consider the integrated luminosity $\mathcal{L}_{\text{int}}$ necessary to produce 10 events as a function of the Z_R mass As can be seen from Fig. B.2 the mass reach of the LHC for 300fb^{-1} (1000fb^{-1}) of integrated luminosity is around 5.5 TeV (7.2 TeV) approximately.

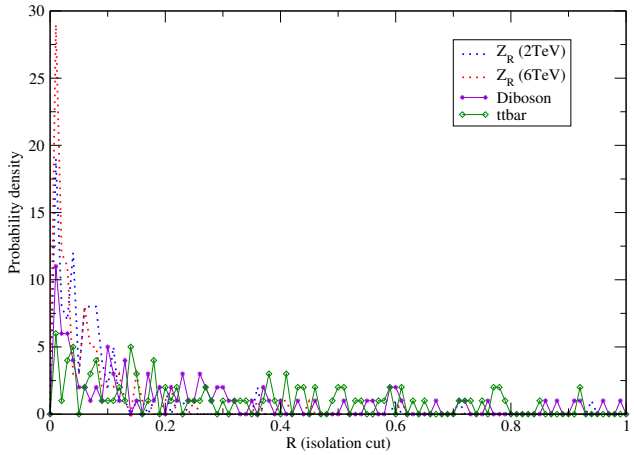

Figure B.1: Probability density as a function of the isolation cut R.

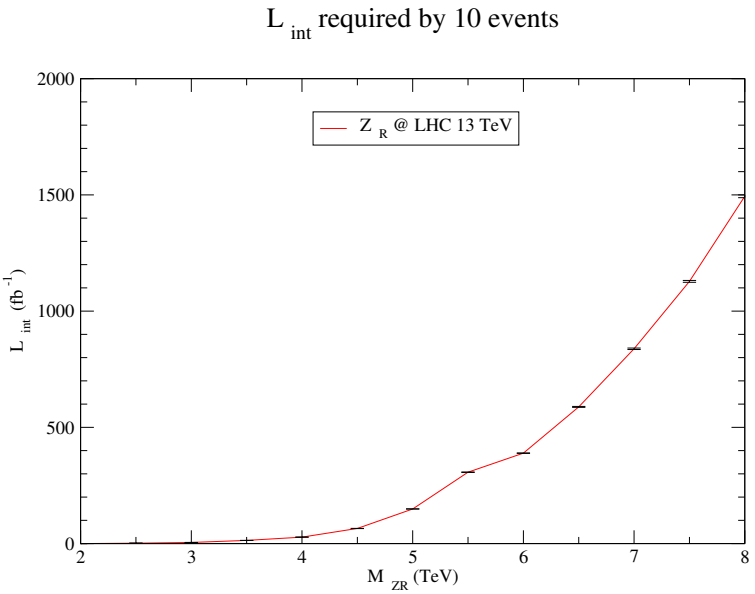

Figure B.2: Values of the integrated luminosity $\mathcal{L}_{\text{int}}$ (fb^{-1}) necessary to produce 10 events as a function of the Z_R mass in TeV. Error bars for $\mathcal{L}_{\text{int}}$ are also shown in the plot.

Appendix C

Expressions for the Dirac phase δ in the right-handed leptonic mixing matrix

In this appendix we present the complete expressions for $\cos\delta$, which is one of the parameters that measures CP violation in the right-handed leptonic mixing matrix V_R. We do it in both two and three heavy neutrinos accessible at the LHC. Furthermore we give the conditions that lead to the maximal allowed value for the phase δ, all in terms of measurable quantities at the LHC.

- Two heavy neutrinos case: In this case we find that the expression 3.13 is given in terms of the physical quantities $\{R_1, R_2, R_\tau, R_4\}$ by the following expression:

$$\begin{aligned}\cos\delta = [&R_1((-2R_\tau + \sqrt{\tfrac{c^{(2)}}{c^{(1)}}R_4} - 1))R_\tau - R_2(\sqrt{\tfrac{c^{(2)}}{c^{(1)}}R_4} - 1))(\sqrt{\tfrac{c^{(2)}}{c^{(1)}}R_4} - R_\tau))(R_\tau + 1)))) + \\ &R_\tau(\sqrt{\tfrac{c^{(2)}}{c^{(1)}}R_4}(R_\tau + R_2(2R_\tau - \sqrt{\tfrac{c^{(2)}}{c^{(1)}}R_4} + 1)))) - R_\tau))]/ \\ &[2R_2\sqrt{1 - \frac{1}{\sqrt{\frac{c^{(2)}}{c^{(1)}}R_4+1}}}(\sqrt{\tfrac{c^{(2)}}{c^{(1)}}R_4} + 1))^{3/2}R_\tau(R_\tau + R_1(R_\tau + 1))))) \\ &\sqrt{-\frac{(R_2\sqrt{\frac{c^{(2)}}{c^{(1)}}R_4} - (R_2+1))R_\tau))(R_2\sqrt{\frac{c^{(2)}}{c^{(1)}}R_4}(R_\tau+1)) - R_\tau))}{R_2^2(\sqrt{\frac{c^{(2)}}{c^{(1)}}R_4}+1))^2R_\tau^2}}\sqrt{\frac{R_\tau + R_1(1 - \frac{R_\tau}{\sqrt{\frac{c^{(2)}}{c^{(1)}}R_4}}))}{R_\tau + R_1(R_\tau+1))}}]\end{aligned} \tag{C.1}$$

  We find two rather simple limiting cases for which $\cos\delta$ vanishes, one is taking $\frac{c^{(2)}}{c^{(1)}}R_4 \to 1$ and $R_1 = R_2$ and the other is taking $\frac{c^{(2)}}{c^{(1)}}R_4 \to 1$ and $R_\tau = 0$ and it this implies that the phase $\delta = \frac{2n+1}{2}\frac{\pi}{2}$, with $n \in \mathbb{Z}$.

- Three heavy neutrinos case: For three HN at the LHC the expression for $\cos\delta$ of Eq. 3.13

is given by:

$$\cos\delta = [(R_2^2 R_3(\sqrt{\tfrac{c^{(2)}}{c^{(1)}}R_4}-1)(\sqrt{\tfrac{c^{(2)}}{c^{(1)}}R_4}+1)^2 + R_2(R_3^2 - 2\sqrt{\tfrac{c^{(2)}}{c^{(1)}}R_4}R_3+1)(\sqrt{\tfrac{c^{(2)}}{c^{(1)}}R_4}+1) +$$
$$R_3(\sqrt{\tfrac{c^{(2)}}{c^{(1)}}R_4}-1))R_1^2 - R_2\sqrt{\tfrac{c^{(2)}}{c^{(1)}}R_4}(R_2(\tfrac{c^{(2)}}{c^{(1)}}R_4+\sqrt{\tfrac{c^{(2)}}{c^{(1)}}R_4})R_3^2 - 2(R_2(\sqrt{\tfrac{c^{(2)}}{c^{(1)}}R_4}+1) +$$
$$(\sqrt{\tfrac{c^{(2)}}{c^{(1)}}R_4}-1)R_3 + R_2(\tfrac{c^{(2)}}{c^{(1)}}R_4+\sqrt{\tfrac{c^{(2)}}{c^{(1)}}R_4}))R_1 + R_2^2R_3(\sqrt{\tfrac{c^{(2)}}{c^{(1)}}R_4}-1)\tfrac{c^{(2)}}{c^{(1)}}R_4]/$$
$$[2R_1R_2(R_3-1)\sqrt{\frac{(1-\frac{\frac{\sqrt{\frac{c^{(2)}}{c^{(1)}}R_4}}{R_1}+\frac{1}{R_2}-1}{\frac{\sqrt{\frac{c^{(2)}}{c^{(1)}}R_4}+1}{R_3-1}})(\frac{\sqrt{\frac{c^{(2)}}{c^{(1)}}R_4}}{R_1}+\frac{1}{R_2}-1)}{\frac{\sqrt{\frac{c^{(2)}}{c^{(1)}}R_4}+1}{R_3-1}}}(\sqrt{\tfrac{c^{(2)}}{c^{(1)}}R_4}+1)^{3/2}$$
$$(R_1(R_2(\sqrt{\tfrac{c^{(2)}}{c^{(1)}}R_4}+1)-R_3) - R_2R_3\sqrt{\tfrac{c^{(2)}}{c^{(1)}}R_4})\sqrt{-\frac{R_3(R_1(R_2(\sqrt{\frac{c^{(2)}}{c^{(1)}}R_4}+1)-1)-R_2\sqrt{\frac{c^{(2)}}{c^{(1)}}R_4})}{R_2R_3\sqrt{\frac{c^{(2)}}{c^{(1)}}R_4}-R_1(R_2(\sqrt{\frac{c^{(2)}}{c^{(1)}}R_4}+1)-R_3)}}$$
$$\sqrt{\frac{\sqrt{\frac{c^{(2)}}{c^{(1)}}R_4}}{\sqrt{\frac{c^{(2)}}{c^{(1)}}R_4}+1}}] \tag{C.2}$$

As in the previous case and by direct inspection of Eq. C.2, we find simple conditions that lead the maximal value for the phase δ. For instance in this case we find three limiting cases for which $\cos\delta \to 0$. The first limiting case is obtained $\frac{c^{(2)}}{c^{(1)}}R_4 \to 1$ and $R_3 = 1$. The second limiting case is obtained by taking $\frac{c^{(2)}}{c^{(1)}}R_4 \to 1$ and $R_1 = R_2$ as in the 2 HN case. Finally the third case is for $\frac{c^{(2)}}{c^{(1)}}R_4 \to 1$ and $R_2 \to 0$.

Processes	Cross section σ[fb] $m_{N_2} = 1$ TeV $m_{N_1} = 100$GeV	$m_{N_1} = 500$GeV	$m_{N_1} = 750$GeV	$m_{N_1} = 950$GeV
$pp \to W_R^+ \to N_1 e^+ \to e^+ e^+ jj$	1.78	1.57	1.44	1.39
$pp \to W_R^+ \to N_1 e^+ \to e^+ \mu^+ jj$	0.61	0.54	0.50	0.48
$pp \to W_R^+ \to N_1 e^+ \to e^+ \tau^+ jj$	0.3	0.27	0.25	0.24
$pp \to W_R^+ \to N_1 e^+ \to \mu^+ \mu^+ jj$	0.21	0.19	0.17	0.16
$pp \to W_R^+ \to N_2 e^+ \to e^+ e^+ jj$	0.33	0.33	0.32	0.32
$pp \to W_R^+ \to N_2 e^+ \to e^+ \mu^+ jj$	0.28	0.28	0.28	0.28
$pp \to W_R^+ \to N_2 e^+ \to \mu^+ \mu^+ jj$	0.25	0.24	0.25	0.25

Table D.1: Cross sections for the different processes considered for two heavy neutrinos at the LHC in the normal hierarchy (NH) neutrino mass spectrum and for different values of the lightest heavy neutrino mass.

Appendix D

Cross sections values

In this appendix we present the results for the cross sections obtained from Madgraph 5 [77] and Pythia 6 [78], for different values of the heavy neutrino masses that we used for generation of the relevant processes at the partonic level and the subsequent hadronization effects.

Processes	Cross section σ[fb] $m_{N_2} = 0.17$ TeV $m_{N_1} = 80$GeV	$m_{N_1} = 100$GeV	$m_{N_1} = 130$GeV	$m_{N_1} = 160$GeV
$pp \to W_R^+ \to N_1 e^+ \to e^+ e^+ jj$	1.61	1.65	1.63	1.68
$pp \to W_R^+ \to N_1 e^+ \to e^+ \mu^+ jj$	0.55	0.57	0.56	0.58
$pp \to W_R^+ \to N_1 e^+ \to \mu^+ \mu^+ jj$	0.19	0.19	0.19	0.20
$pp \to W_R^+ \to N_2 e^+ \to e^+ e^+ jj$	0.42	0.42	0.43	0.43
$pp \to W_R^+ \to N_2 e^+ \to e^+ \mu^+ jj$	0.36	0.36	0.38	0.37
$pp \to W_R^+ \to N_2 e^+ \to \mu^+ \mu^+ jj$	0.31	0.32	0.33	0.32
$pp \to W_R^+ \to N_3 e^+ \to e^+ \mu^+ jj$	0.048	0.024	0.026	0.027
$pp \to W_R^+ \to N_3 e^+ \to \mu^+ \mu^+ jj$	1.6	0.80	0.85	89

Table D.2: Cross sections for the different processes considered for three heavy neutrinos at the LHC in the normal hierarchy (NH) neutrino mass spectrum and for different values of the lightest heavy neutrino mass.

Processes	Cross section σ[fb] $m_{N_2} = 0.95$ TeV $m_{N_3} = 80$GeV	$m_{N_3} = 100$GeV	$m_{N_3} = 300$GeV	$m_{N_3} = 500$GeV
$pp \to W_R^+ \to N_1 e^+ \to e^+ e^+ jj$	1.35	1.34	1.32	1.36
$pp \to W_R^+ \to N_1 e^+ \to e^+ \mu^+ jj$	0.46	0.46	0.45	0.47
$pp \to W_R^+ \to N_1 e^+ \to \mu^+ \mu^+ jj$	0.16	0.16	0.16	0.16
$pp \to W_R^+ \to N_2 e^+ \to e^+ e^+ jj$	0.34	0.35	0.34	0.34
$pp \to W_R^+ \to N_2 e^+ \to e^+ \mu^+ jj$	0.29	0.30	0.29	0.29
$pp \to W_R^+ \to N_2 e^+ \to \mu^+ \mu^+ jj$	0.25	0.26	0.25	0.26
$pp \to W_R^+ \to N_3 e^+ \to e^+ \mu^+ jj$	0.027	0.028	0.026	0.026
$pp \to W_R^+ \to N_3 e^+ \to \mu^+ \mu^+ jj$	0.92	0.91	0.85	0.86

Table D.3: Cross sections for the different processes considered for three heavy neutrinos at the LHC in the inverted hierarchy (IH) neutrino mass spectrum and for different values of the lightest heavy neutrino mass.

Appendix E

Branching ratio formulas for $\delta_R^{++} \to l^+ l^+$

In this appendix we show the explicit formulas for the branching ratios $\mathrm{Br}(\delta_R^{++} \to e^+e^+)$, $\mathrm{Br}(\delta_R^{++} \to \mu^+e^+)$ and $\mathrm{Br}(\delta_R^{++} \to \mu^+\mu^+)$,

$$\mathrm{Br}(\delta_R^{++} \to e^+e^+) = \frac{1}{\sum_k m_{N_k}^2} |c_{13}^2 c_{12}^2 m_{N_1} + e^{-2i\phi_2} c_{13}^2 s_{12}^2 m_{N_2} + e^{-2i(\phi_3-\delta)} s_{13}^2 m_{N_3}^2|^2, \tag{E.1}$$

$$\begin{aligned}\mathrm{Br}(\delta_R^{++} \to e^+\mu^+) =& \frac{2}{\sum_k m_{N_k}^2} |(-s_{12}c_{23} - c_{12}s_{23}s_{13}e^{-i\delta}) c_{12}c_{13} m_{N_1} + \\ & (c_{12}c_{23} - s_{12}s_{23}s_{13}e^{-i\delta}) s_{12}c_{13} e^{-2i\phi_2} m_{N_2} + s_{23}c_{13}s_{13}e^{-i(2\phi_3-\delta)} m_{N_3}|^2,\end{aligned} \tag{E.2}$$

$$\begin{aligned}\mathrm{Br}(\delta_R^{++} \to \mu^+\mu^+) =& \frac{1}{\sum_k m_{N_k}^2} |(-s_{12}c_{23} - c_{12}s_{23}s_{13}e^{-i\delta})^2 m_{N_1} + \\ & (c_{12}c_{23} - s_{12}s_{23}s_{13}e^{-i\delta})^2 e^{-2i\phi_2} m_{N_2} + s_{23}^2 c_{13}^2 e^{-2i\phi_3} m_{N_3}|^2.\end{aligned} \tag{E.3}$$

Notice that this branching ratios are independent of the doubly-charged scalar masses and depend only on the masses of the heavy neutrinos

Appendix F

Kinematics of the $\mu \to e\gamma$ process and the triple vector correlation

In this appendix we give some tools that could be useful when computing the triple vector correlation shown in Eq. (4.7) for the $\mu \to e\gamma$ decay.

For the anti-muon we use the spinor $v(p_{\mu^+})$ given by

$$v(p_{\mu^+}) = \begin{pmatrix} \sqrt{p\cdot\sigma} & \xi \\ -\sqrt{p\cdot\bar{\sigma}} & \xi \end{pmatrix}, \tag{F.1}$$

where $\xi^\dagger\xi = 1$ and p_{μ^+} is given in Eq. (4.3). As shown in Fig. 2.1 the polarization vector of the muon is given by:

$$\vec{s} = |\vec{s}|(\sin\Phi\cos\Psi, \sin\Phi\sin\Psi, \cos\Phi) \tag{F.2}$$

and it is straightforward to show that in this case

$$\xi^n = \begin{pmatrix} e^{-i\frac{\Psi}{2}}\cos\frac{\Phi}{2} \\ e^{i\frac{\Psi}{2}}\sin\frac{\Phi}{2} \end{pmatrix}. \tag{F.3}$$

One may find the same result by requiring ξ to be an eigenvector of $\vec{\sigma}\cdot\hat{n}$, where $\hat{n}$ is a unitary vector in the direction of $\vec{s}$.

For the electron and for the reference frame shown in Fig.2.1 we use

$$v_{e^+}(p_{e^+}) = \sqrt{\frac{|\vec{p}_{e^+}|}{2}} \begin{pmatrix} -2e^{i\frac{\theta_s}{2}}\sin\frac{\theta_s}{2} \\ 2ie^{-i\frac{\theta_s}{2}}\sin\frac{\theta_s}{2} \\ 2ie^{i\frac{\theta_s}{2}}\cos\frac{\theta_s}{2} \\ -2e^{-i\frac{\theta_s}{2}}\cos\frac{\theta_s}{2} \end{pmatrix}. \tag{F.4}$$

The photon has two possible polarizations along the direction of motion and in the particular frame we are considering in Fig.2.1 its polarization vector is given by,

$$\epsilon^{\mu}_{\pm}(p_\gamma) = \frac{1}{\sqrt{2}} \begin{pmatrix} 0 \\ \pm i\cos\theta_s \\ \mp i\sin\theta_s \\ 1 \end{pmatrix} \tag{F.5}$$

where we can explicitly see that when $\theta_s = 0$, the photon can only have a polarization ± 1 along the y-axis and p_γ and p_{e^+} are the 4-momentum of the outgoing photon and electron respectively – see Eq. (4.4) and (4.5). Once the expressions for the spinors of the participating fermions and the polarization vector of the photon are known, it is easy straightforward to compute the triple vector asymmetry given in (4.7).

We found that the total decay rate is given by

$$\Gamma_{\text{total}} = \frac{2}{\pi} G_F^2 m_\mu^5 e^2 (|A_L|^2 + |A_R|^2). \tag{F.6}$$

It would be interesting to compare the above equation with the result one gets when summing the decay rates for $\cos\Phi > 0$ to that of $\cos\Phi < 0$, namely

$$\Gamma(\cos\Phi > 0) + \Gamma(\cos\Phi < 0) = \frac{2}{\pi} G_F^2 m_\mu^5 e^2 (\cos^2\frac{\theta_s}{2}|A_L|^2 + \sin^2\frac{\theta_s}{2}|A_R|^2). \tag{F.7}$$

On the other hand, by subtracting the total decay rates for $\cos\Phi > 0$ to that of $\cos\Phi < 0$ one gets:

$$\Gamma(\cos\Phi > 0) - \Gamma(\cos\Phi < 0) = \frac{2}{\pi} G_F^2 m_\mu^5 e^2 \sin\theta_s \Im m(A_L A_R^*) \tag{F.8}$$

from which the asymmetry shown in (4.7) can be readily computed. It should be noted that the asymmetry is obtained for linearly polarized photons, i.e. photons with linear polarization in the $\hat{p}_e \times \hat{p}_e$ direction. This is the crucial point since it means that one can put the experimental setup such that $\hat{p}_e$ and $\hat{s}_e$ both lie in a given plane. Then one can trigger the event by requiring that together with a signal one must see a photon in the $\hat{p}_e \times \hat{p}_e$ direction after the linear polarizing device.

Bibliography

[1] Jogesh C. Pati and Abdus Salam. Lepton Number as the Fourth Color. Phys. Rev., D10:275–289, 1974. [Erratum: Phys. Rev.D11,703(1975)].

[2] Rabindra N. Mohapatra and Jogesh C. Pati. Left-Right Gauge Symmetry and an Isoconjugate Model of CP Violation. Phys. Rev., D11:566–571, 1975.

[3] R. N. Mohapatra and Jogesh C. Pati. A Natural Left-Right Symmetry. Phys. Rev., D11:2558, 1975.

[4] G. Senjanović and Rabindra N. Mohapatra. Exact Left-Right Symmetry and Spontaneous Violation of Parity. Phys. Rev., D12:1502, 1975.

[5] Goran Senjanović. Spontaneous Breakdown of Parity in a Class of Gauge Theories. Nucl. Phys., B153:334–364, 1979.

[6] Miha Nemevsek, Goran Senjanović, and Vladimir Tello. Connecting Dirac and Majorana Neutrino Mass Matrices in the Minimal Left-Right Symmetric Model. Phys. Rev. Lett., 110(15):151802, 2013.

[7] Peter Minkowski. $\mu \to e\gamma$ at a Rate of One Out of 10^9 Muon Decays? Phys. Lett., B67:421–428, 1977.

[8] Rabindra N. Mohapatra and Goran Senjanović. Neutrino Mass and Spontaneous Parity Violation. Phys. Rev. Lett., 44:912, 1980.

[9] Rabindra N. Mohapatra and Goran Senjanović. Neutrino Masses and Mixings in Gauge Models with Spontaneous Parity Violation. Phys. Rev., D23:165, 1981.

[10] S. Glashow. Quarks and leptons, Cargése 1979, ed. M. Lévy (Plenum, NY, 1980); M. Gell-Mann et al., Supergravity Stony Brook workshop, New York, 1979.

[11] R. Slansky P. Ramond. Supergravity Stony Brook work- shop New York, 1979, ed. P. Van Niewenhuizen, D. Free- man (North Holland, Amsterdam, 1980).

[12] T. Yanagida. Workshop on unifed theories and baryon number in the universe, ed. A. Sawada, A. Sugamoto (KEK, Tsukuba, 1979).

[13] G. Senjanović. Neutrino mass: From LHC to grand unification. Riv. Nuovo Cim., 34:1–68, 2011.

[14] Goran Senjanović. Seesaw at LHC through Left - Right Symmetry. Int. J. Mod. Phys., A26:1469–1491, 2011.

[15] Vladimir Tello. Connections Between the High and Low Energy Violation of Lepton and Flavor Numbers in the Minimal Left-Right Symmetric Model . PhD thesis.

[16] Wai-Yee Keung and Goran Senjanović. Majorana Neutrinos and the Production of the Right-handed Charged Gauge Boson. Phys. Rev. Lett., 50:1427, 1983.

[17] Goran Senjanović and Vladimir Tello. Right Handed Quark Mixing in Left-Right Symmetric Theory. Phys. Rev. Lett., 114(7):071801, 2015.

[18] Andrew Fowlie and Luca Marzola. Testing quark mixing in minimal leftâĂŞright symmetric models with b -tags at the LHC. Nucl. Phys., B889:36–45, 2014.

[19] J. Adam et al. New constraint on the existence of the $\mu^+ \to e^+\gamma$ decay. Phys. Rev. Lett., 110:201801, 2013.

[20] Wilhelm H. Bertl et al. A Search for muon to electron conversion in muonic gold. Eur. Phys. J., C47:337–346, 2006.

[21] Andre de Gouvea and Niki Saoulidou. Fermilab's intensity frontier. Ann. Rev. Nucl. Part. Sci., 60:513–538, 2010.

[22] J. Miller, V. S. Kashikhin, D. V. Neuffer, C. M. Ankenbrandt, R. P. Johnson, C. Y. Yoshikawa, and R. A. Rimmer. Intense Muon Beams for Experiments at Project X. Conf. Proc., C110328:1951–1953, 2011.

[23] H. Witte et al. Status of the PRISM FFAG Design for the Next Generation Muon-to-Electron Conversion Experiment. Conf. Proc., C1205201:79–81, 2012.

[24] S. Mihara, J. P. Miller, P. Paradisi, and G. Piredda. Charged Lepton Flavor-Violation Experiments. Ann. Rev. Nucl. Part. Sci., 63:531–552, 2013.

[25] Yasaman Farzan. Tracing CP-violation in lepton flavor violating muon decays. JHEP, 07:054, 2007.

[26] Seyed Yaser Ayazi and Yasaman Farzan. A Window on the CP-violating Phases of MSSM from Lepton Flavor Violating Processes. JHEP, 01:022, 2009.

[27] Lincoln Wolfenstein. Final state interactions and CP violation in weak decays. Phys. Rev., D43:151–156, 1991.

[28] Borut Bajc, Miha Nemevsek, and Goran Senjanović. Probing leptonic CP phases in LFV processes. Phys. Lett., B684:231–235, 2010.

[29] Juan Carlos Vasquez. Right-handed lepton mixings at the LHC. JHEP, 05:176, 2016.

[30] Juan Carlos Vasquez. Time-reversal symmetry violation in several Lepton-Flavor-Violating processes. JHEP, 09:131, 2015.

[31] N. G. Deshpande, J. F. Gunion, Boris Kayser, and Fredrick I. Olness. Left-right symmetric electroweak models with triplet Higgs. Phys. Rev., D44:837–858, 1991.

[32] Yue Zhang, Haipeng An, Xiangdong Ji, and Rabindra N. Mohapatra. General CP Violation in Minimal Left-Right Symmetric Model and Constraints on the Right-Handed Scale. Nucl. Phys., B802:247–279, 2008.

[33] Ken Kiers, Michael Assis, and Alexey A. Petrov. Higgs sector of the left-right model with explicit CP violation. Phys. Rev., D71:115015, 2005.

[34] Alessio Maiezza, Miha NemevÅąek, and Fabrizio Nesti. Perturbativity and mass scales of Left-Right Higgs bosons. 2016.

[35] Wouter Dekens and Daniel Boer. Viability of minimal leftâĂŞright models with discrete symmetries. Nucl. Phys., B889:727–756, 2014.

[36] W. Dekens. Testing left-right symmetric models. In Proceedings, 50th Rencontres de Moriond Electroweak interactions and unified theories, pages 515–518, 2015.

[37] Miha Nemevsek, Goran Senjanović, and Vladimir Tello. Work to appear.

[38] Goran SenjanoviÄĞ and Vladimir Tello. Restoration of Parity and the Right-Handed Analog of the CKM Matrix. 2015.

[39] G. Beall, Myron Bander, and A. Soni. Constraint on the Mass Scale of a Left-Right Symmetric Electroweak Theory from the K(L) K(S) Mass Difference. Phys. Rev. Lett., 48:848, 1982.

[40] Alessio Maiezza, Miha Nemevsek, Fabrizio Nesti, and Goran Senjanović. Left-Right Symmetry at LHC. Phys. Rev., D82:055022, 2010.

[41] Stefano Bertolini, Alessio Maiezza, and Fabrizio Nesti. Present and Future K and B Meson Mixing Constraints on TeV Scale Left-Right Symmetry. Phys. Rev., D89(9):095028, 2014.

[42] Alessio Maiezza and Miha NemevÅąek. Strong P invariance, neutron electric dipole moment, and minimal left-right parity at LHC. Phys. Rev., D90(9):095002, 2014.

[43] Vardan Khachatryan et al. Search for heavy neutrinos and W bosons with right-handed couplings in proton-proton collisions at $\sqrt{s} = 8\,\text{TeV}$. Eur. Phys. J., C74(11):3149, 2014.

[44] Serguei Chatrchyan et al. Search for heavy neutrinos and W[R] bosons with right-handed couplings in a left-right symmetric model in pp collisions at sqrt(s) = 7 TeV. Phys. Rev. Lett., 109:261802, 2012.

[45] Georges Aad et al. Search for anomalous production of prompt same-sign lepton pairs and pair-produced doubly charged Higgs bosons with $\sqrt{s} = 8$ TeV *pp* collisions using the ATLAS detector. JHEP, 03:041, 2015.

[46] J. A. Casas and A. Ibarra. Oscillating neutrinos and muon —> e, gamma. Nucl. Phys., B618:171–204, 2001.

[47] Pavel Fileviez Perez, Tao Han, Gui-yu Huang, Tong Li, and Kai Wang. Neutrino Masses and the CERN LHC: Testing Type II Seesaw. Phys. Rev., D78:015018, 2008.

[48] Alejandra Melfo, Miha Nemevsek, Fabrizio Nesti, Goran Senjanović, and Yue Zhang. Type II Seesaw at LHC: The Roadmap. Phys. Rev., D85:055018, 2012.

[49] J. S. Bell and R. Jackiw. A PCAC puzzle: pi0 –> gamma gamma in the sigma model. Nuovo Cim., A60:47–61, 1969.

[50] Stephen L. Adler. Axial vector vertex in spinor electrodynamics. Phys. Rev., 177:2426–2438, 1969.

[51] Gerard 't Hooft. Symmetry Breaking Through Bell-Jackiw Anomalies. Phys. Rev. Lett., 37:8–11, 1976.

[52] Y. Fukuda et al. Evidence for oscillation of atmospheric neutrinos. Phys. Rev. Lett., 81:1562–1567, 1998.

[53] Q. R. Ahmad et al. Measurement of the rate of $\nu_e + d \to p + p + e^-$ interactions produced by ^8B solar neutrinos at the Sudbury Neutrino Observatory. Phys. Rev. Lett., 87:071301, 2001.

[54] K. Eguchi et al. First results from KamLAND: Evidence for reactor anti-neutrino disappearance. Phys. Rev. Lett., 90:021802, 2003.

[55] P. A. R. Ade et al. Planck 2015 results. XIII. Cosmological parameters. 2015.

[56] M. C. Gonzalez-Garcia, Michele Maltoni, Jordi Salvado, and Thomas Schwetz. Global fit to three neutrino mixing: critical look at present precision. JHEP, 12:123, 2012.

[57] Bernard Aubert et al. Searches for Lepton Flavor Violation in the Decays tau+- —> e+- gamma and tau+- —> mu+- gamma. Phys. Rev. Lett., 104:021802, 2010.

[58] J. P. Lees et al. Limits on tau Lepton-Flavor Violating Decays in three charged leptons. Phys. Rev., D81:111101, 2010.

[59] Bernard Aubert et al. Search for Lepton Flavor Violating Decays tau —> l- K0(s) with the BABAR Experiment. Phys. Rev., D79:012004, 2009.

[60] Bernard Aubert et al. Search for lepton flavor violating decays tau+- —> l+- omega (l = e, mu). Phys. Rev. Lett., 100:071802, 2008.

[61] Bernard Aubert et al. Search for Lepton Flavor Violating Decays $\tau^\pm \to \ell^\pm\pi^0$, $\ell^\pm\eta$, $\ell^\pm\eta'$. Phys. Rev. Lett., 98:061803, 2007.

[62] T. Aushev et al. Physics at Super B Factory. 2010.

[63] T. Abe et al. Belle II Technical Design Report. 2010.

[64] A. M. Baldini et al. MEG Upgrade Proposal. 2013.

[65] M. Aoki. An experimental search for muon-electron conversion in nuclear field at sensitivity of 10**-14 with a pulsed proton beam. AIP Conf. Proc., 1441:599–601, 2012.

[66] Hiroaki Natori. DeeMe experiment - An experimental search for a mu-e conversion reaction at J-PARC MLF. Nucl. Phys. Proc. Suppl., 248-250:52–57, 2014.

[67] U. Bellgardt et al. Search for the Decay mu+ —> e+ e+ e-. Nucl. Phys., B299:1–6, 1988.

[68] A. Blondel et al. Research Proposal for an Experiment to Search for the Decay $\mu \to eee$. 2013.

[69] S. Weinberg and G. Feinberg. Electromagnetic Transitions Between mu Meson and Electron. Phys. Rev. Lett., 3:111–114, 1959.

[70] W. J. Marciano and A. I. Sanda. The Reaction mu- Nucleus –> e- Nucleus in Gauge Theories. Phys. Rev. Lett., 38:1512, 1977.

[71] Oruganti U. Shanker. Z Dependence of Coherent μe Conversion Rate in Anomalous Neutrinoless Muon Capture. Phys. Rev., D20:1608, 1979.

[72] Ryuichiro Kitano, Masafumi Koike, and Yasuhiro Okada. Detailed calculation of lepton flavor violating muon electron conversion rate for various nuclei. Phys. Rev., D66:096002, 2002. [Erratum: Phys. Rev.D76,059902(2007)].

[73] M. E. Rose, L. C. Biedenharn, and G. B. Arfken. Internal conversion angular correlations. Phys. Rev., 85:5–16, Jan 1952.

[74] M. E. Rose. Relativistic electron theory. 1961.

[75] T. S. Kosmas, Sergey Kovalenko, and Ivan Schmidt. Nuclear muon- e- conversion in strange quark sea. Phys. Lett., B511:203, 2001.

[76] S. P. Das, F. F. Deppisch, O. Kittel, and J. W. F. Valle. Heavy Neutrinos and Lepton Flavour Violation in Left-Right Symmetric Models at the LHC. Phys. Rev., D86:055006, 2012.

[77] J. Alwall, R. Frederix, S. Frixione, V. Hirschi, F. Maltoni, O. Mattelaer, H. S. Shao, T. Stelzer, P. Torrielli, and M. Zaro. The automated computation of tree-level and next-to-leading order differential cross sections, and their matching to parton shower simulations. JHEP, 07:079, 2014.

[78] Torbjorn Sjostrand, Stephen Mrenna, and Peter Z. Skands. PYTHIA 6.4 Physics and Manual. JHEP, 05:026, 2006.

[79] A. Ferrari, Johann Collot, M-L. Andrieux, B. Belhorma, P. de Saintignon, J-Y. Hostachy, Ph. Martin, and M. Wielers. Sensitivity study for new gauge bosons and right-handed Majorana neutrinos in pp collisions at s = 14-TeV. Phys. Rev., D62:013001, 2000.

[80] S. N. Gninenko, M. M. Kirsanov, N. V. Krasnikov, and V. A. Matveev. Detection of heavy Majorana neutrinos and right-handed bosons. Phys. Atom. Nucl., 70:441–449, 2007.

[81] Miha Nemevˇsek, Fabrizio Nesti, Goran Senjanović, and Yue Zhang. First Limits on Left-Right Symmetry Scale from LHC Data. Phys. Rev., D83:115014, 2011.

[82] Chien-Yi Chen, P. S. Bhupal Dev, and R. N. Mohapatra. Probing Heavy-Light Neutrino Mixing in Left-Right Seesaw Models at the LHC. Phys. Rev., D88:033014, 2013.

[83] P. S. Bhupal Dev, Doojin Kim, and Rabindra N. Mohapatra. Disambiguating Seesaw Models using Invariant Mass Variables at Hadron Colliders. JHEP, 01:118, 2016.

[84] Shrihari Gopalakrishna, Tao Han, Ian Lewis, Zong-guo Si, and Yu-Feng Zhou. Chiral Couplings of W' and Top Quark Polarization at the LHC. Phys. Rev., D82:115020, 2010.

[85] Tao Han, Ian Lewis, Richard Ruiz, and Zong-guo Si. Lepton Number Violation and W' Chiral Couplings at the LHC. Phys. Rev., D87(3):035011, 2013. [Erratum: Phys. Rev.D87,no.3,039906(2013)].

[86] S. Coleman and R. E. Norton. Singularities in the physical region. Nuovo Cim., 38:438–442, 1965.

[87] Tao Han and Yingchuan Li. Genuine CP-odd Observables at the LHC. Phys. Lett., B683:278–281, 2010.

[88] Aviad Roitgrund, Gad Eilam, and Shaouly Bar-Shalom. Implementation of the left-right symmetric model in FeynRules/CalcHep. 2014.

[89] Vladimir Tello, Miha Nemevsek, Fabrizio Nesti, Goran Senjanović, and Francesco Vissani. Left-Right Symmetry: from LHC to Neutrinoless Double Beta Decay. Phys. Rev. Lett., 106:151801, 2011.

[90] Miha Nemevsek, Fabrizio Nesti, Goran Senjanović, and Vladimir Tello. Neutrinoless Double Beta Decay: Low Left-Right Symmetry Scale? 2011.

[91] J. de Favereau, C. Delaere, P. Demin, A. Giammanco, V. LemaÃőtre, A. Mertens, and M. Selvaggi. DELPHES 3, A modular framework for fast simulation of a generic collider experiment. JHEP, 02:057, 2014.

[92] Eric Conte, Benjamin Fuks, and Guillaume Serret. MadAnalysis 5, A User-Friendly Framework for Collider Phenomenology. Comput. Phys. Commun., 184:222–256, 2013.

[93] Vardan Khachatryan et al. Reconstruction and identification of ÏĎ lepton decays to hadrons and Î¡ at CMS. JINST, 11(01):P01019, 2016.

[94] K. Huitu, J. Maalampi, A. Pietila, and M. Raidal. Doubly charged Higgs at LHC. Nucl. Phys., B487:27–42, 1997.

[95] A. G. Akeroyd and Mayumi Aoki. Single and pair production of doubly charged Higgs bosons at hadron colliders. Phys. Rev., D72:035011, 2005.

[96] Georges Azuelos, K. Benslama, and J. Ferland. Prospects for the search for a doubly-charged Higgs in the left-right symmetric model with ATLAS. J. Phys., G32(2):73–91, 2006.

[97] A. G. Akeroyd, Mayumi Aoki, and Hiroaki Sugiyama. Probing Majorana Phases and Neutrino Mass Spectrum in the Higgs Triplet Model at the CERN LHC. Phys. Rev., D77:075010, 2008.

[98] Tao Han, Biswarup Mukhopadhyaya, Zongguo Si, and Kai Wang. Pair production of doubly-charged scalars: Neutrino mass constraints and signals at the LHC. Phys. Rev., D76:075013, 2007.

[99] G. Bambhaniya, J. Chakrabortty, J. Gluza, T. JeliÅĎski, and M. Kordiaczynska. Lowest limits on the doubly charged Higgs boson masses in the minimal left-right symmetric model. Phys. Rev., D90(9):095003, 2014.

[100] J. Chakrabortty, J. Gluza, R. Sevillano, and R. Szafron. Left-Right Symmetry at LHC and Precise 1-Loop Low Energy Data. JHEP, 07:038, 2012.

[101] Margarete Muhlleitner and Michael Spira. A Note on doubly charged Higgs pair production at hadron colliders. Phys. Rev., D68:117701, 2003.

[102] G. Bambhaniya, J. Chakrabortty, J. Gluza, M. KordiaczyÅĎska, and R. Szafron. Left-Right Symmetry and the Charged Higgs Bosons at the LHC. JHEP, 05:033, 2014.

[103] A. D. Martin, W. J. Stirling, R. S. Thorne, and G. Watt. Parton distributions for the LHC. Eur. Phys. J., C63:189–285, 2009.

[104] CMS Collaboration. Inclusive search for doubly charged Higgs in leptonic final states with the 2011 data at 7 TeV. 2012.

[105] F. Corriveau, J. Egger, W. Fetscher, H. J. Gerber, K. F. Johnson, H. Kaspar, H. J. Mahler, M. Salzmann, and F. Scheck. DOES THE POSITRON FROM MUON DECAY HAVE TRANSVERSE POLARIZATION? Phys. Lett., B129:260–264, 1983.

[106] H. Burkard, F. Corriveau, J. Egger, W. Fetscher, H. J. Gerber, K. F. Johnson, H. Kaspar, H. J. Mahler, M. Salzmann, and F. Scheck. Muon Decay: Measurement of the Transverse Positron Polarization and General Analysis. Phys. Lett., B160:343–348, 1985.

[107] Kai U. Kohler. Determination of the polarization vector of positrons from the decay of polarized muons.

[108] W. Fetscher et al. Polarized muon decay: Measurement of the polarization vector of the decay positrons as a test of time reversal invariance. Nucl. Phys., A721:457–460, 2003.

[109] W. Fetscher et al. Measurement of the polarization vector of the e+ from the decay of polarized mu+ as a test of time reversal invariance. J. Phys., G29:2017–2020, 2003.

[110] R. A. Mann and M. E. Rose. Depolarization of Negative mu Mesons. Phys. Rev., 121:293–301, 1961.

[111] V. Cirigliano, A. Kurylov, M. J. Ramsey-Musolf, and P. Vogel. Lepton flavor violation without supersymmetry. Phys. Rev., D70:075007, 2004.

[112] Goran Senjanović and Pavao Senjanovic. Suppression of Higgs Strangeness Changing Neutral Currents in a Class of Gauge Theories. Phys. Rev., D21:3253, 1980.

[113] Joydeep Chakrabortty, H. Zeen Devi, Srubabati Goswami, and Sudhanwa Patra. Neutrinoless double-β decay in TeV scale Left-Right symmetric models. JHEP, 08:008, 2012.

[114] Frank F. Deppisch, Martin Hirsch, and Heinrich Pas. Neutrinoless Double Beta Decay and Physics Beyond the Standard Model. J. Phys., G39:124007, 2012.

[115] James Barry and Werner Rodejohann. Lepton number and flavour violation in TeV-scale left-right symmetric theories with large left-right mixing. JHEP, 09:153, 2013.

[116] Chang-Hun Lee, P. S. Bhupal Dev, and R. N. Mohapatra. Natural TeV-scale left-right seesaw mechanism for neutrinos and experimental tests. Phys. Rev., D88(9):093010, 2013.

[117] P.âĂĽS. Bhupal Dev, Srubabati Goswami, and Manimala Mitra. TeV Scale Left-Right Symmetry and Large Mixing Effects in Neutrinoless Double Beta Decay. Phys. Rev., D91(11):113004, 2015.

[118] T. Suzuki, David F. Measday, and J. P. Roalsvig. Total Nuclear Capture Rates for Negative Muons. Phys. Rev., C35:2212, 1987.

[119] ATLAS sensitivity prospects to WâĂš and ZâĂš in the decay channels WâĂš->lnu and ZâĂš->l+l- at sqrt(s)=7 TeV. 2010.

[120] Frank F. Deppisch, Tomas E. Gonzalo, Sudhanwa Patra, Narendra Sahu, and Utpal Sarkar. Signal of Right-Handed Charged Gauge Bosons at the LHC? Phys. Rev., D90(5):053014, 2014.

[121] J. A. Aguilar-Saavedra and F. R. Joaquim. Closer look at the possible CMS signal of a new gauge boson. Phys. Rev., D90(11):115010, 2014.

[122] Matti Heikinheimo, Martti Raidal, and Christian Spethmann. Testing Right-Handed Currents at the LHC. Eur. Phys. J., C74(10):3107, 2014.

[123] Janusz Gluza and Tomasz JeliÅĎski. Heavy neutrinos and the ppâĘŠlljj CMS data. Phys. Lett., B748:125–131, 2015.

[124] Bogdan A. Dobrescu and Zhen Liu. WâĂš Boson near 2 TeV: Predictions for Run 2 of the LHC. Phys. Rev. Lett., 115(21):211802, 2015.

[125] Pilar Coloma, Bogdan A. Dobrescu, and Jacobo Lopez-Pavon. Right-handed neutrinos and the 2 TeV W' boson. Phys. Rev., D92(11):115023, 2015.

[126] Triparno Bandyopadhyay, Biswajoy Brahmachari, and Amitava Raychaudhuri. Implications of the CMS search for W_R on grand unification. JHEP, 02:023, 2016.

[127] P. S. Bhupal Dev and R. N. Mohapatra. Unified explanation of the $eejj$, diboson and dijet resonances at the LHC. Phys. Rev. Lett., 115(18):181803, 2015.

[128] Johann Brehmer, JoAnne Hewett, Joachim Kopp, Thomas Rizzo, and Jamie Tattersall. Symmetry Restored in Dibosons at the LHC? JHEP, 10:182, 2015.

[129] Alessio Maiezza, Miha NemevÅąek, and Fabrizio Nesti. Lepton Number Violation in Higgs Decay at LHC. Phys. Rev. Lett., 115:081802, 2015.

[130] P. S. Bhupal Dev, Rabindra N. Mohapatra, and Yongchao Zhang. Probing the Higgs Sector of the Minimal Left-Right Symmetric Model at Future Hadron Colliders. JHEP, 05:174, 2016.

[131] J. Chakrabortty, J. Gluza, T. Jelinski, and T. Srivastava. Theoretical constraints on masses of heavy particles in Left-Right Symmetric Models. Phys. Lett., B759:361–368, 2016.